Bulletin de l'Institut Scientifique, Rabat, Section Sciences de la Terre, 2018, n° 40, 91-113. ***e-ISSN : 2458-7184***

The Tafilalt magmatic complex (Eastern Anti Atlas, Morocco): New insights into petrology and geochemistry; and preliminary interpretation

Le complexe magmatique du Tafilalt (Anti-Atlas Est, Maroc) : Nouvelles données pétrographiques et géochimiques ; interprétation préliminaire

Amine NAJIH[1*] Abdelilah FEKKAK[1], Hassan EZZOUHAIRI[1], Lahssen BAIDDER[2], Ilyass BERRADA[1], Brahim KARAOUI[3] & Abdelkader MAHMOUDI[4]

1. Department of Geology, Sciences Faculty, Chouaib Doukkali University, BP. 20, 24000 El Jadida, Morocco. * (*aminenajih24@gmail.com*)
2. Faculty of Sciences Ain Chock, Hassan II University, Casablanca, Morocco.
3. Faculty of Sciences and Technics, Moulay Ismaïl University, BP. 509, 52000 Errachidia; Morocco
4. Faculty of Sciences, Moulay Ismaïl University, BP. 11201, Meknes, Morocco

Abstract. In the eastern Moroccan Anti-Atlas, the Tafilalt Province exposes folded Cambrian-Visean series intruded by a number of dykes, sills and laccoliths. These intrusions constitute the Tafilalt Magmatic Complex, TMC. New field, petrographic and geochemical data from the TMC provide an opportunity to decipher the nature of their sources and approach their geotectonic significance. Three petrographic facies have been recognized, i.e., olivine dolerites in some of the sills, kaersutite-bearing lamprophyres occurring in dykes and sills, and eventually gabbro-syenites in the laccoliths. The olivine dolerites are composed of olivine, pyroxene, plagioclase and kaersutite. Geochemically, they show high values of MgO, Mg#, Cr and Ni indicating a genesis with a minor fractionation in olivine and clinopyroxene. Geochemical data of these rocks include high LREE with $(La/Yb)_{Pm}$ ≈2.44 with no Eu anomalies and a discrete negative Ti anomaly. The kaersutite lamprophyres (dykes and sills) and the gabbro-syenites (laccoliths) contain low percentages in olivine and pyroxene, but display abundant kaersutite and high Fe/Mg content. The analyzes show more or less similar values in MgO, Mg#, Cr, Ni and high LREE values with $(La/Yb)_{Pm}$≈6.86. They share geochemical characteristics in Sr and Ti anomalies indicating a fractionation of plagioclase and ferro-titanium oxides. All the TMC rocks display a high-Ti OIB alkaline character and show ratios $(Gd/Yb)_C > 2$ and $Ti/Y \geq 500$ which attest for a genesis from mantle plume. The TMC rocks cannot be ascribed to any Devonian-Carboniferous magmatism for structural reasons. They differ geochemically from the tholeiitic intrusions of the Central Atlantic Magmatic Province. They have to be ascribed to a post-Visean and pre-Triassic magmatic event.

Keywords: Anti-Atlas, Tafilalt, Magmatism, Plume, High-Ti, Late Paleozoic.

Résumé. A l'extrémité orientale de l'Anti Atlas marocain, la province de Tafilalt expose des séries plissées cambro-viséennes intrusives par un certain nombre de dykes, sills et laccolithes. Ces intrusions constituent le complexe magmatique de Tafilalt, CMT. Les données pétrographiques du CMT permettent d'examiner la nature de leurs sources. Selon le mode de gisement, trois faciès de roche se distinguent. Les dolérites à olivine reconnues dans certains sills, les lamprophyres à kaersutite répandus dans les dykes et sills et un dernier consistant en gabbro et syénite dans les laccolithes. Les dolérites à olivine - sills groupe1 se composent par des cristaux d'olivine, pyroxène, plagioclase et kaersutite. Géochimiquement, ils présentent des valeurs élevées en MgO, Mg#, Cr et Ni indiquant une genèse avec un fractionnement mineur en olivine et clinopyroxène. Les données géochimiques pour ces roches incluent des valeurs en LREE élevées avec $(La/Yb)_{Pm}$≈2.44, avec aucune anomalie en Eu et une anomalie négative discrète en Ti. Les lamprophyres à kaersutite (dykes et sills groupe2) et les gabbros-syénites (laccolithes) contiennent de faibles pourcentages en olivine et pyroxène mais présentent une abondance en kaersutite et ferromagnésiens, les analyses chimiques montrent des valeurs plus ou moins similaires en MgO, Mg#, Cr, Ni et des valeurs élevées LREE avec $(La/Yb)_{Pm}$≈6.86. Ils partagent des caractéristiques géochimiques en anomalies négatives en Sr et Ti indiquant un fractionnement des plagioclases et oxides ferro-titanés. Toutes les roches du CMT affichent un caractère alcalin de type OIB riche en Ti et se positionnent des rapports en $(Gd/Yb)_C$ >2 et $Ti/Y \geq 500$ qui plaident pour une genèse à partir d'un panache mantellique. Le magmatisme TMC ne peut être rattachés structuralement au Dévono-Carbonifère, ni géochimiquement au CAMP. Il est fort probablement lié à un événement fini-Paléozoïque qui serait post-Viséen et anté-Triasique.

Mots-clés. Anti-Atlas, Tafilalt, Magmatisme, Panache, Riche en Ti, Fini Paléozoïque.

INTRODUCTION

The Anti-Atlas is a thick-skinned Variscan belt showing Precambrian inliers beneath a mildly folded Paleozoic cover (Fig.1). At the eastern tip of the belt, i.e., in the Tafilalt region, the lower Cambrian to Carboniferous folded series are intruded by a number of mafic dykes, sills and laccoliths (Destombes & Hollard 1986, Álvaro *et al*. 2014a, Benharref *et al*. 2014b-c-d, Pouclet *et al*. 2017).

These intrusions are locally secant on the Ordovician-Early Carboniferous formations and are widespread in the form of sills within the Silurian, Devonian and Tournaisian-Visean formations. A complex of laccoliths occurs locally in the Famennian formations and at the Devonian-Carboniferous interface. The age of this post-Ordovician magmatism is controversial. Pouclet *et al*. (2017) ascribed the post-Ordovician dolerites to two pre-Variscan events, Devonian and Carboniferous, respectively, while Chabou *et*

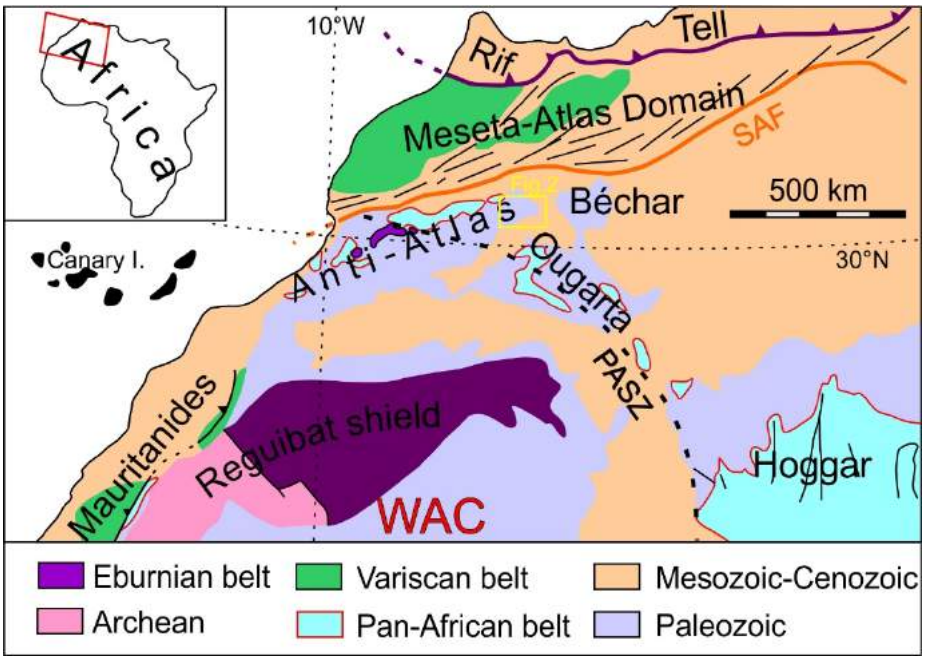

Figure 1. Structural context of the northern West African Craton (WAC) after Michard et al. (2017). PASZ: Pan-African suture zone; SAF: South Atlas fault.

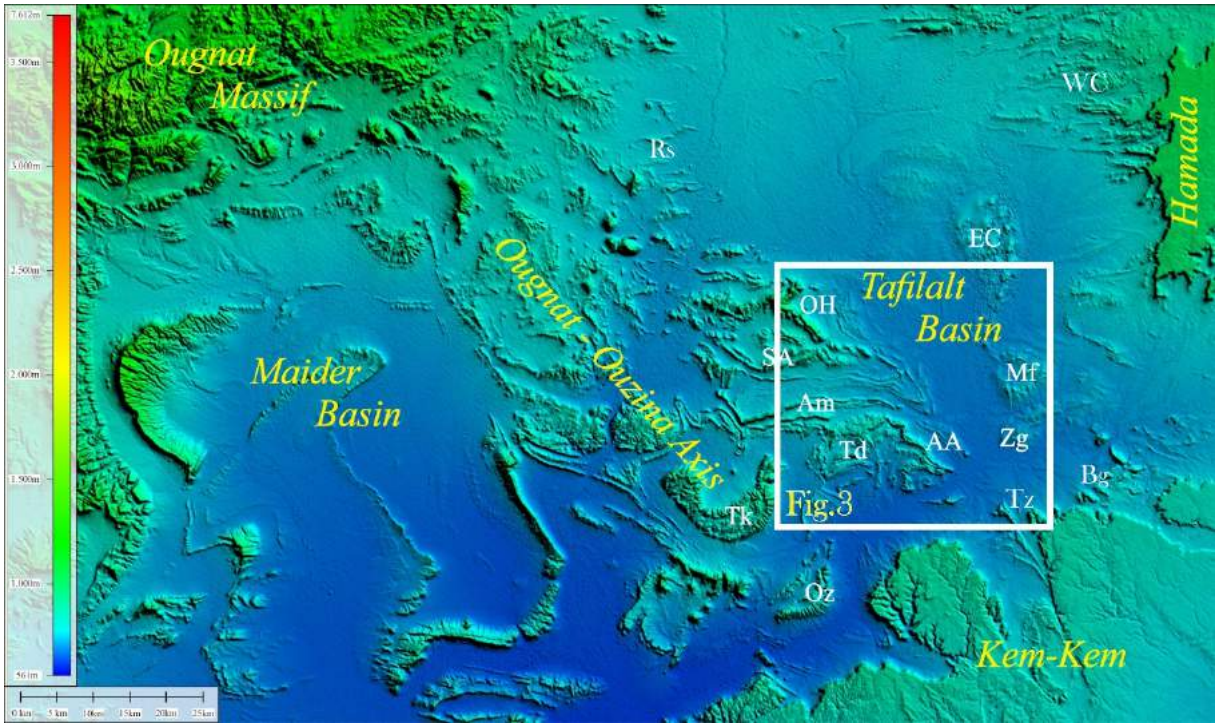

Figure 2. Digital Elevation Model of the Eastern Anti-Atlas with main structural domains, major folds and localities. EC: Erg Chebbi (Merzouga dunes), Mf: Mfis, Zg: Znaigui folds, AA: Al Atrous, Td: Tadaout, Am: Amessoui, SA: Sheib Arras, OH: Oum Hdej, Tk: Tijkhet, Oz: Ouzina, Rs: Rissani, WC: Widane Chebbi, Tz: Tawz, Bg: Begaa. Framed: Figure. 3.

al. (2017a-b) suggested a single event that would be post-Variscan, although being distinct from, and likely older than the Central Atlantic Magmatic Province (CAMP) event (ca. 200 Ma; Sebai *et al*. 1991, Youbi *et al*. 2003, Verati *et al*. 2007, Davies *et al*. 2017).

In this article, we present an analysis of the geochemical data available (Álvaro *et al*. 2014a, Benharref *et al*. 2014a-b-c, Pouclet *et al*. 2017) or obtained during the present work in order to check the uniqueness or plurality of their origin and to discuss their potential source and emplacement mechanism.

GEOLOGICAL SETTING

The Tafilalt is located at the junction between the Anti-Atlas and Ougarta ranges (Fig. 1). Belonging to the eastern

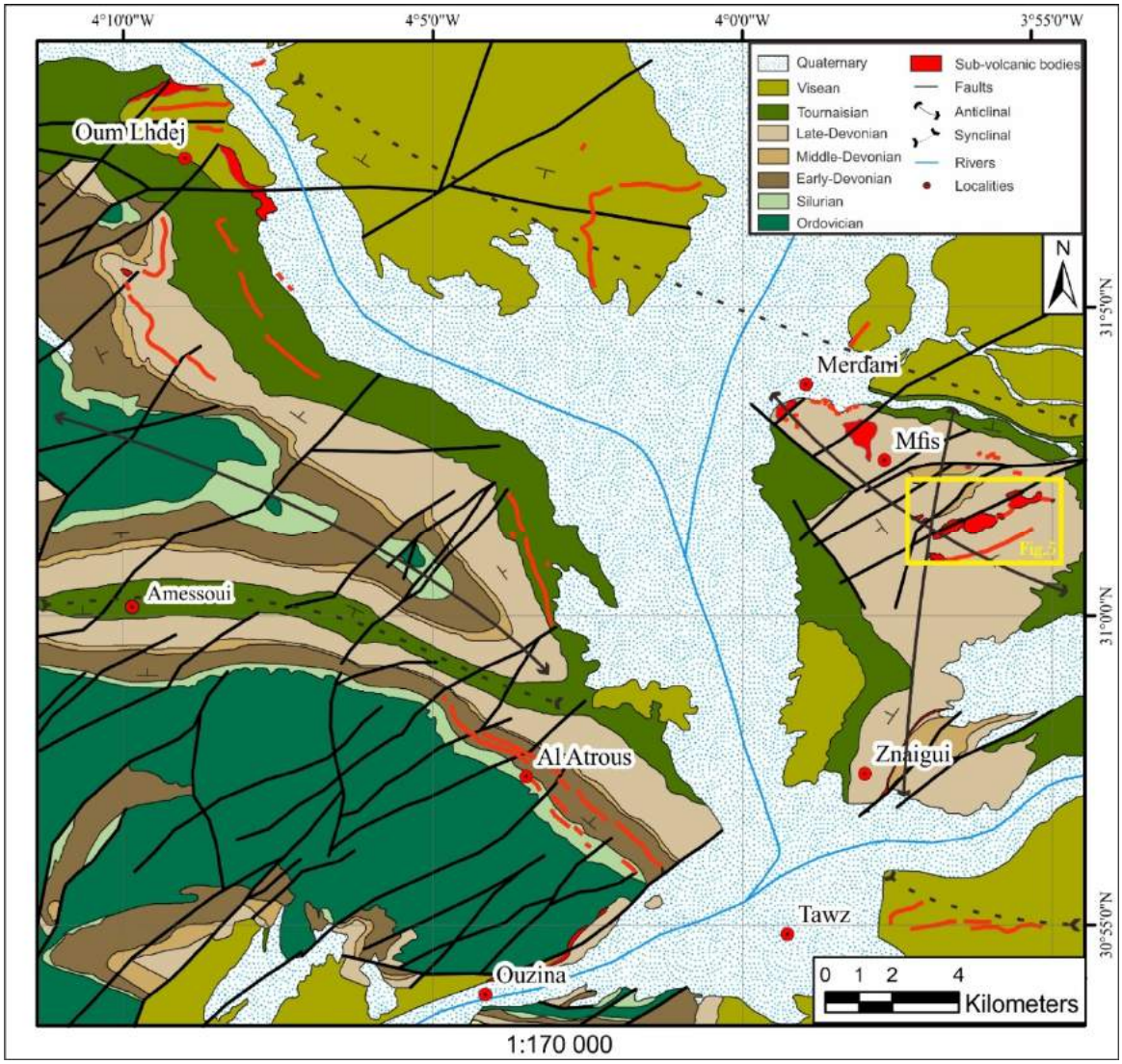

Figure 3. Geological map of the study area, generated from maps of Álvaro *et al*. (2014a), Benharref *et al*. (2014a), Koukaya *et al*. (2014) and Tahiri *et al*. (2014).

tip of the Anti-Atlas, the Tafilalt Paleozoic units are limited in the north by the Cretaceous deposits of the sub-Atlas zone, in the south by those of the Kem-Kem plateau, in the east by the Meso-Cenozoic Hamada of Guir, and in the west by the Ougnat-Ouzina Axis and the Maider basin (Fig. 2). The Tafilalt Paleozoic series rest on a Neoproterozoic substratum, which crops out in the Ougnat massif and to the NE of Erfoud, as well as to the SW of Ouzina (Fig. 2). They range from the Early Cambrian to the end of the Early Carboniferous. This sequence is mainly made of sandstones, pelites and shales in the Lower Paleozoic, with increasing proportion of limestones, marls, and calcareous sandstones from the Silurian upward (Figures 3, 4) (Hollard 1974 et 1981; Wendt 1985 et 1988, Destombes *et al*. 1986; Baidder *et al*. 2007, 2008, 2016, Clerc *et al*. 2013, Álvaro *et al*. 2014a, Benharref *et al*. 2014b-c-d). The Tafilalt region is slightly deformed and belongs to the external domain of the Hercynian belt whose metamorphic internal domain develops in the Atlas-Meseta domain further to the north (Michard *et al*. 2010). The Paleozoic rocks are organized in a succession of anticlines and synclines with frequent sigmoidal or even boomerang axial trajectories. These forms have been interpreted as the result of polyphase Hercynian deformation and control of fault blocks (Baidder *et al*. 2016). The anticlines of the Ougnat-Ouzina Axis show Cambrian and Ordovician terrains, whereas those of the Tafilalt basin, such as the Znaigui or Mfis (Dboa) anticlines,expose Devonian units, and the synclines (such as Amessoui or Marzouga synclines) preserve the Devonian and Carboniferous units (Fig. 3). The magmatic event here studied is essentially represented by a multitude of doleritic dykes and sills schematically shown in Fig. 4. In the area particularly studied here (Fig. 3), the sills become particularly thick and are labeled laccoliths near Mfis (Dboa laccolith; Pouclet *et al*. 2017).

TAFILALT MAGMATIC COMPLEX:

Field relationships:

The Tafilalt magmatic complex consists of dykes, sills and laccoliths. The main, first-order feeder dykes that have

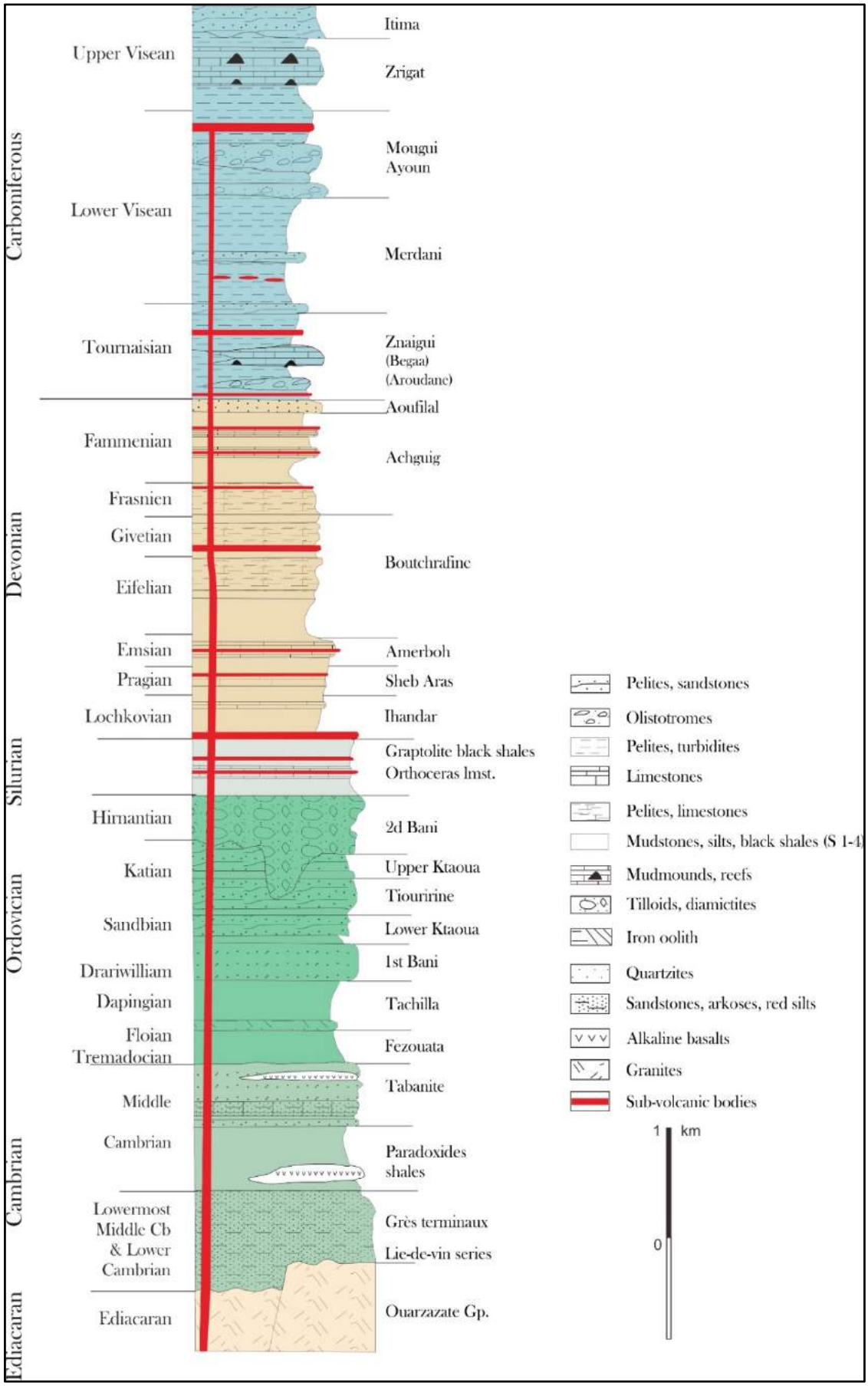

Figure 4. Generalized stratigraphic column of the Tafilalt region adapted from Baidder *et al*. (2016).

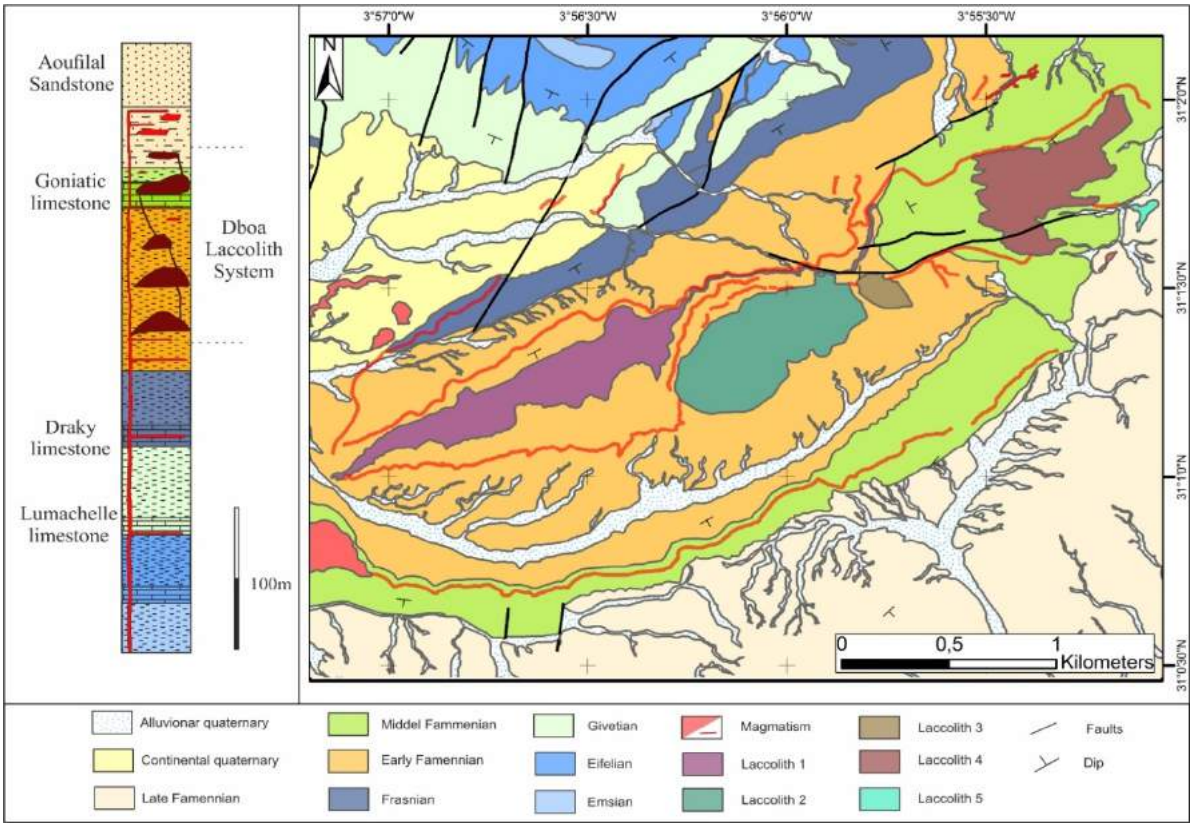

Figure 5. Geological map and stratigraphic column of the Dboa laccoliths system, after the Geological map of Morocco scale 1:50.000, Mfis quadrangle, and this work.

several kilometers length. These dykes follow km-scale fault zones such as the Ouzina, Znaigui and Mfis faults (Figures. 3, 5). Their magmatic material is brecciated and rich in xenoliths and phenocrysts, especially biotite (Fig. 6A-B). The second-order feeder dykes show lesser dimensions, with a few meters to a few tens of meters lengthiness. They are more frequent and ensure vertical communication between sills and laccoliths (Fig. 6C). The second-order dykes may contain fragments of reworked first-order dykes (Fig. 6D) (see below), which indicates the existence of two magmatic pulsations. The sills are of unequal importance, their thickness vary from <1 m to 20 m locally, even along the same sill. They are mostly localized in the weakness zones between incompetent and competent layers (e.g., Silurian shales or Visean marly-pelites on the one hand, limestone or sandstone beds on the other hand) (Fig. 6E). A sill can change laterally its position in the stratigraphic pile, especially in a thick marly series where rheology and space are favorable. The most illustrative case of this phenomenon is observed in the marls of the Emsian along the Wadi Al Atrous (4°01'26"W, 30°56'00'N) (Fig. 6F) where the sill is inserted along the Emsian limestone (d3a)-Emsian marls (d3b) interface and laterally crosses the Emsian marls to extend along the Emsian marl-Eifelian limestone interface (d4). The petrography of the sills is constant whatever the stratigraphic level of emplacement. The laccolith architecture is observed in two areas: (i) in the Znaigui area, where two second-order feeder dykes originate from a first-order dyke through the Znaigui fault, feeding a mushroom-shaped laccolith that is emplaced at the base of the lower Famennian marls (d7a) (Fig. 6D-G-H); (ii) in the Jbel Dboa in the core of the Mfis anticline, which exposes a laccolithic complex of five interconnected laccoliths laterally superimposed in staircase setting (Figures 5, 7, 8). The lower laccolith is hosted by the marls of the Early Famennian (d7a) and the upper one occurs in the shales of the Aoufilal Formation (d7c). The laccolith 1 (LA1) intrudes the base of the Famennian at about twenty meters above the Frasnian-Famennian boundary. It extends on 1.9 km long with a thickness of 120 m in its axial part. Several second-order feeding dykes start from laccolith 1 to feed laccolith 2 (LA2). The LA2 is shifted laterally relative to the LA1 and occupies the middle part of the Early Famennian marls (d7a). Its lateral extension exceeds 820 m, while its thickness reaches 80 m in its axial part. LA3 is a small laccolith (212m over 115m in size) which occupies the top part of the Famennian marl (d7a) and corresponds to a satellite of LA2. The LA3 has, however, connections with the LA2 and LA4 laccoliths. The latter has the same importance as the LA1 and the LA2 and is set up in the upper part of the Famennian goniatite limestones (d7b). LA4 is 930 m long and 539 m wide. The last laccolith LA5 occurs in the basal and shaly part of the Aoufilal Formation (d7c). It is relatively small (150m over 32m) and fed by a dyke linking it to LA4.

Petrography

In this section, we study the petrography of the TMC according to type of intrusion (dykes, sills and laccoliths).

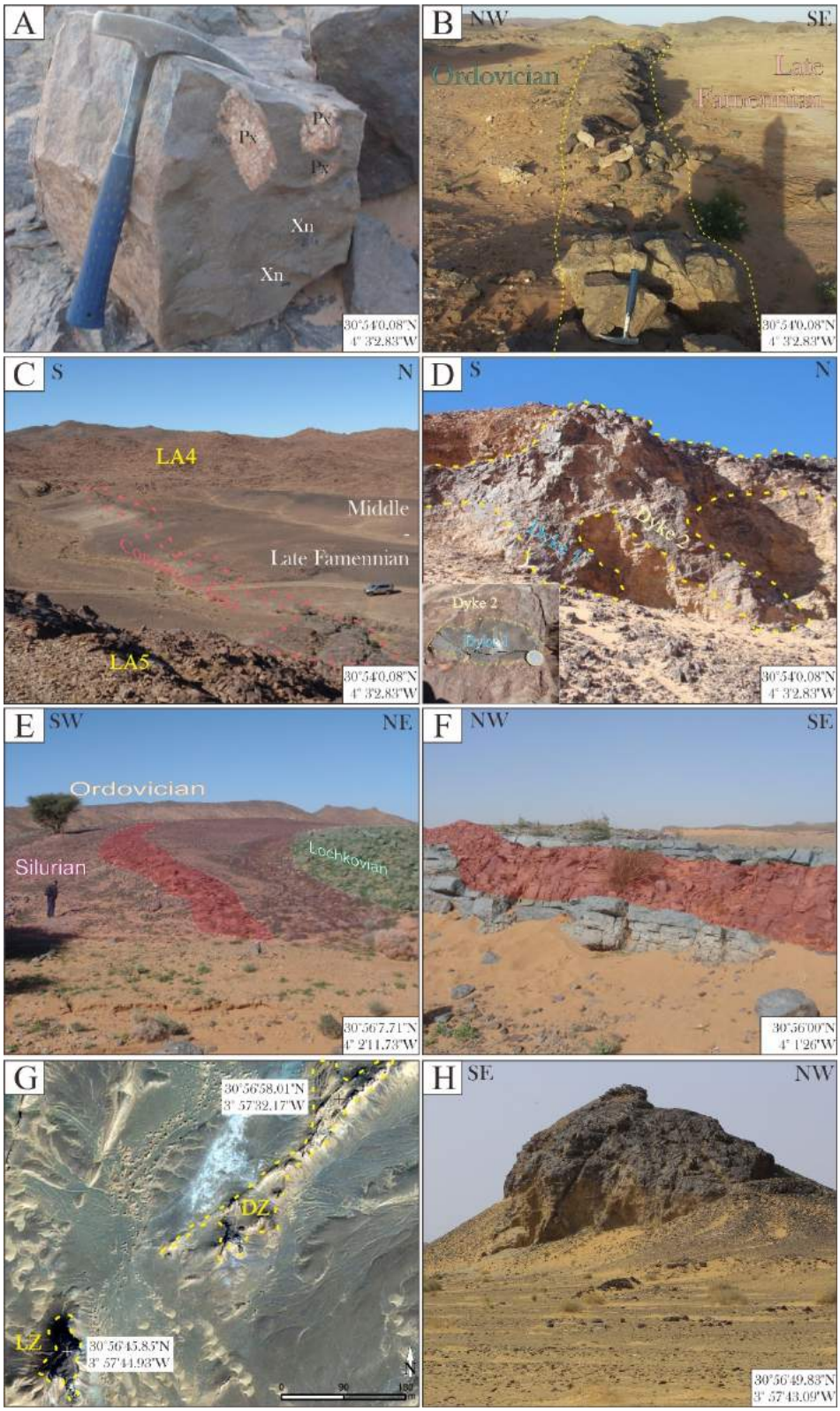

Figure 6. (A) Ouzina dyke with enclave; Xn: Xenoliths, Px: Phenocrysts. (B) Feeder dyke. (C) Connection dyke between two laccoliths (LA 4, LA5). (D) Interaction between two feeder dykes; fragment of dyke1 is seen as xenolith in dyke2, pulled off and carried in the ascending dyke 2. (E) Sill in the Silurian-Devonian interface. (F) Sill intersecting obliquely the Emsian limestones. (G) Sub-volcanic Znaigui system; LZ: Znaigui laccolith, DZ : Znaigui dyke. (H) Znaigui laccolith.

The TMC supply system is provided by first-order dykes that follow the main faults of the sector (Ouzina, Znaigui and Mfis faults). These dykes can feed sills and laccoliths directly. Feeding can also be done through second-order dykes feeding themselves from first-order dykes. Brecciation is a common character to all dykes. However, this character is more pronounced in the first-order dykes than in the second-order ones. On the other hand, first-order dykes are richer in xenocrysts of biotite, feldspar and quartz. They are also richer in volcanoclastic and plutonic enclaves probably uprooted from the Ediacarian substratum (Fig. 6A). Petrographically, the dykes are kaersutite lamprophyres showing microdoleritic to fluidal texture. They are composed mainly by plagioclase and kaersutite phenocrysts

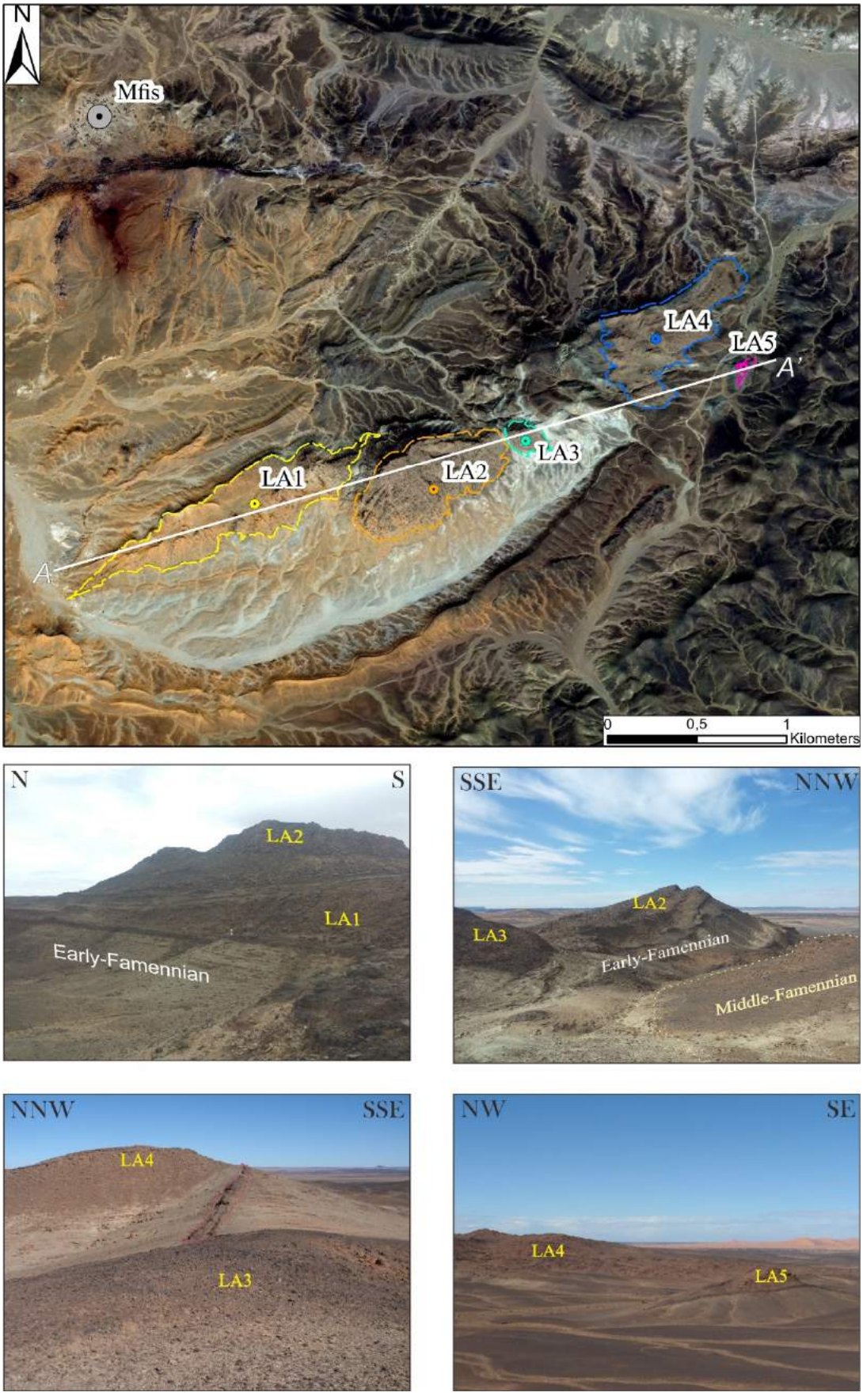

Figure 7. Dboa laccoliths system with five laccoliths labeled in ascending order LA1-5 (see interpreted satellite image and cross-section Fig. 8).

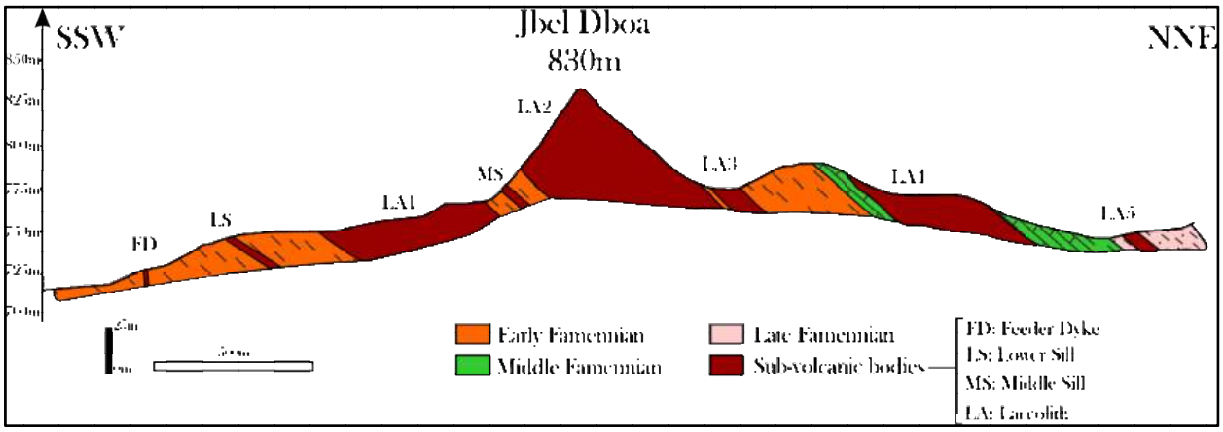

Figure 8. Geological section showing the Dboa laccoliths system.

(<1mm). The groundmass is made by microcrystals of plagioclase and amphibole. The plagioclase fraction is the dominant mineral phase accompanied by opaque minerals. The ferromagnesian minerals present are kaersutite and biotite (Fig. 9A-B). The sills are injected into Paleozoic formations from the Silurian to the Visean. Sills of olivine dolerites have intergranular to intersertal porphyry texture. They show at their core more olivine phenocrysts (0.25 mm<) and clinopyroxene (0.25-0.5 mm) with scarce kaersutite microcrystals (1 mm) (Fig. 9A). The plagioclase crystals (>1.25 mm) are altered into epidote and tiny white mica ("sericite"). Olivines and clinopyroxenes are completely altered into epidote and chlorite. Iron oxides are scattered in the groundmass. At the sill's borders, olivine and clinopyroxene are small and hosted in a fine grained groundmass rich in plagioclase microlites (Fig. 9B). This facies is limited to sills hosted in Silurian to Emsian strata. Sills of kaersutite lamprophyres have an intersertal texture, and olivine percentage is less than 2% (Fig. 9C-D). Olivine and clinopyroxene minerals are partially or totally transformed into calcite, epidote and chlorite. Kaersutite (<1mm) crystals are the most abundant ferromagnesian minerals in thin section. They are usually altered into chlorite and actinolite. Plagioclases subhedral crystals (<1.5mm) are essentially altered into "sericite". The rock is rich in iron oxides. This facies is found at all levels of the Paleozoic pile from Silurian to Visean. The laccoliths have different sizes, but all of them show a fine-grained border and a coarse-grained core. The fine-grained border compares with the kaersutite lamprophyres sills. Gabbros and syenites constitute the core of the laccoliths. The gabbros are composed of pyroxene phenocrysts (<1mm), kaersutite (>1.5mm), biotite (<1mm), alkali feldspar and plagioclase (<1.5mm) (Fig. 9E). The groundmass consists essentially of alkaline feldspars and plagioclases. The secondary minerals present are "sericite", calcite and opaque minerals. The syenites have a microgranular to grained texture (Fig. 9F). These rocks are composed mainly of alkaline feldspar (0.5-1 mm), biotite (<1mm), kaersutite (0.5-1 mm), plagioclase and altered pyroxenes crystals (<1mm). The groundmass consists of alkaline feldspar with more or less apparent plagioclase. The secondary minerals present are calcite, chlorite, opaque minerals, and elongated crystals of apatite. As a whole, petrographic analysis indicates broadly constant lamprophyric facies for the dykes and gabbros and syenites facies for the laccoliths. However, two different groups can be distinguished in the sills according to the petrographic facies: a first group of facies corresponds to olivine-rich dolerites found only in the formations ranging from Silurian to Emsian, whereas a second group of facies corresponds to olivine-poor, kaersutite-rich lamprophyres that are common in the entire Paleozoic series from Silurian to Visean.

Geochemistry

The TMC was concerned by 98 analyses during the PNCG (National Program for Geological Cartography) (Benharref *et al.* 2014, Álvaro *et al.* 2014). These analyses also compiled in Pouclet *et al.* (2017) were done on a large area from Rissani to the west until Widane Chebbi to the east (Fig. 2). We focused on the Marzouga-Mfis key area by carrying out 33 new sample analyses to densify sampling for a better credibility of the results, and also to sample bodies that have not been analyzed in the PNCG such as some laccoliths and dykes. This paper proposes an integrated study of all the available analyzes new ones and PNCG data. The major trace elements and rare earth elements were determined by ICP-MS (inductively coupled plasma and mass spectrometry) at the ACMELABS certified laboratory in Canada. The analysis accuracy of the major and trace elements is less than 1% and 1 -5% respectively. The loss on ignition (LOI) observed in these rocks are related to the presence of hydrated minerals (e.g. kaersutite and biotite), to the low-grade metamorphism and hydrothermal alteration that these rocks have undergone (Pouclet *et al.* 2017). All rocks analyzed are basic and have low SiO_2 contents of 37.91 - 50.45 wt%. They are rich in MgO (from 2.23 to 9.54), Fe_2O_3t (7.61 to 12.94), TiO_2 (1.51 to 3.17) and alkalis ($Na_2O + K_2O$) (of 3.02 to 10.48) with always $Na_2O/K_2O>1$, which gives these rocks a rather sodic character according to Middlemost (1975), but $Na_2O + K_2O$ always remain lower than Al_2O_3. TMC dykes have SiO2 concentration between 40.42 to 46.93%wt, MgO from 4.55 to 8.88%, Fe_2O_3 from 8.94 to 12.94%, TiO_2 from 2.04 to 2.72% and alkali (Na_2O+K_2O) from 3.67 to 6.56%. The olivine dolerite sills belonging to the group 1 defined above have SiO_2 levels ranging from 39.58 to 47.02%, MgO from 4.37 to 8%, Fe_2O_3t from 8.02 to 12.56%, TiO_2 from 1.72. to 3.14% and alkali ($Na_2O + K_2O$) from 3.02 to 6.68% (Tableau). The kaersutite lamprophyres of the group 2 sills have a more or

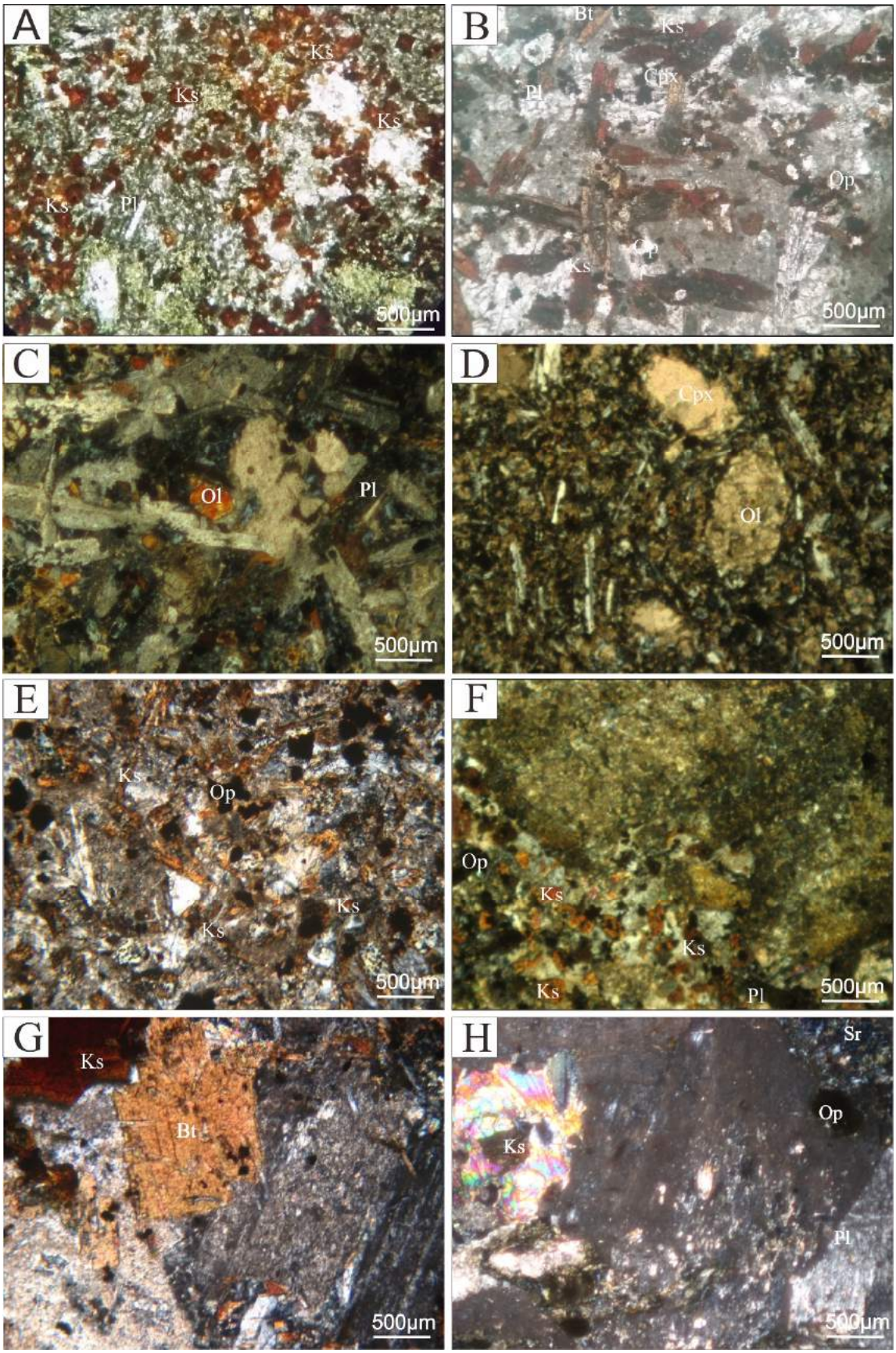

Figure 9. (A&B) Kaersutite lamprophyre dyke, (C&D) Olivine Dolerite; (C) Core facies intergranular to intersertal texture and (D) Microlitic texture border facies, olivine and clinopyroxene relica; (E&F) Kaersutite lamprophyres; (G&H) Coarse grained laccolithic facies; (G) gabbroic facies and (H) syenitic facies. Ol:olivine, Cpx: clinopyroxene, Pl: plagioclase, Ks: kaersutite, Bt:biotite, Sr: sericite, Op : opaque mineral.

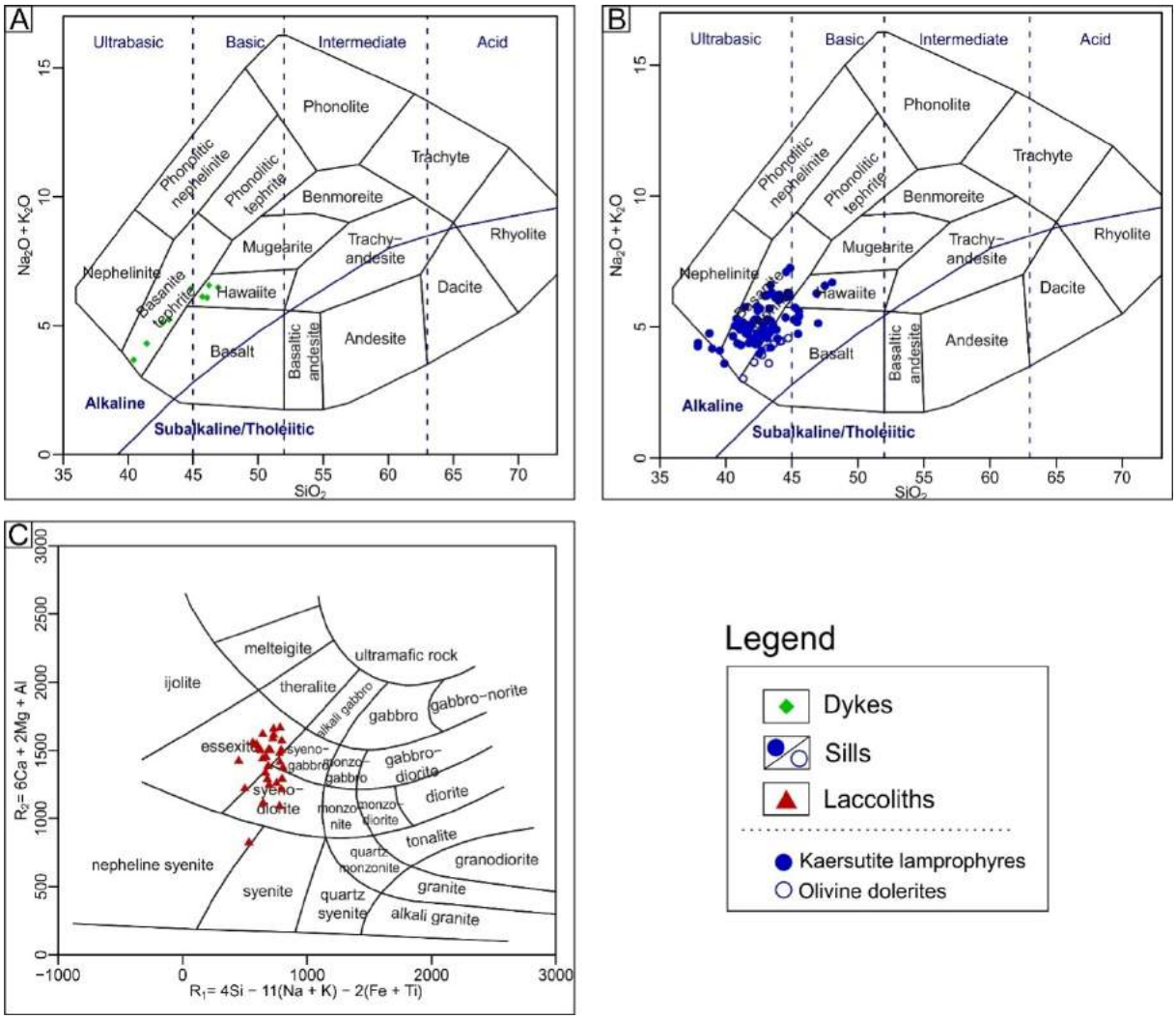

Figure 10. (A&B) Nomenclature diagram SiO_2 vs Na_2O+K_2O after Cox *et al*. (1979) and (C) after De la Roche *et al*. (1980).

less differentiated chemical composition, with SiO_2 levels between 39.03 and 52.93 %, MgO from 2.22 to 7.5%, Fe_2O_3t from 5.14 to 11.5%, TiO_2 from 1.51 to 2.78% and alkali from 4.29 to 10.48%. Laccoliths rocks present chemical concentration of SiO_2 ranging from 39.03 to 52.93%, MgO from 2.22 to 7.5%, Fe_2O_3 from 5.14 to 11.5%, TiO_2 from 1.51 to 2.78% and total alkali ($4.29<Na_2O+K_2O<10.48$ wt%).(Tableau). In the nomenclature diagram (Cox et al. 1979), the dykes occupy basanites-tephrites and hawaites domains (Fig. 10A). As for the sills, the application of the same diagram confirms the distinction between the two petrographic groups. Group 1 sills (olivine dolerites) fall into alkali basalts field, while group 2 sills (kaersutite lamprophyres) mostly plot in the basanite-tephrite field with some in the hawaites and mugearite fields (Fig. 10B). Laccoliths show chemical compositions similar to those of dykes and sills of the petrographic group 2. In the De la Roche *et al*. (1980) diagram (Fig. 10C), they correspond to essexites (monzogabbros, monzodiorites, monzonites and monzosyenites), syenodiorites and syeno-gabbros.

On the other hand, all the TMC rocks display Ti/Y ratios between 427 and 847, generally higher than an average of 500, and allow us to consider them as Ti-rich basalts (Xu *et al.* 2001, Xizo *et al.* 2004, Lai *et al.* 2012). Dykes are characterized by an Mg# (MgO/(MgO+FeO)) between 47-63 with negative Sr (Sr/Sr*=0.71), Ti (Ti/Ti*=0.59) anomalies and positive Eu anomaly (Eu/Eu*=1.05). The $(La/Yb)_{Pm}$ ratio varies between 4.57 and 7.68 with richness in REE (ΣREE=317-557) (Fig. 11). The olivine dolerites of group 1 are characterized by an Mg# between 52-61 with positive Sr (Sr/Sr * = 1.21) and Ti (Ti/Ti * = 0.99) anomalies; a ratio $(La/Yb)_{Pm}$ between 1.4-2.2 and a low abundance of REE (ΣREE = 97 to 174ppm) (Fig. 11). The group 2 sills (kaersutite lamprophyres) are characterized by an Eu (Eu/Eu * = 1.07) and negative anomaliesof Sr (Sr/Sr * = 0.76) and Ti (Ti/Ti * = 0.65), which respectively indicate a significant fractionation of plagioclases and ferro-titanated oxides. They are rich in REE (ΣREE_{avg} = 449ppm) with their large fractionation $(La/Yb)_{Pm}$ between 3.9-10.24 (Fig. 11). The laccoliths have Mg# (43-60), Sr (Sr/Sr*=0.70), Ti (Ti/Ti*=0.53) and Eu(Eu/Eu*=1.07). The laccoliths REE sums areΣREE= 315 – 561 and the ratio $(La/Yb)_{Pm}$ between 4.91 and 8.51 (Fig. 11). The TMC rocks have a Nb and Ta positive anomalies suggesting low crustal participation in the genesis of their fluids, whereas the Zr-Hf positive anomaly for TMC dykes, laccoliths and group 2 sills involves late hydrothermal fluid intervention in the magmatic fluid (Fig. 11) (Roddaz *et al.* 2002, Pouclet *et al.*

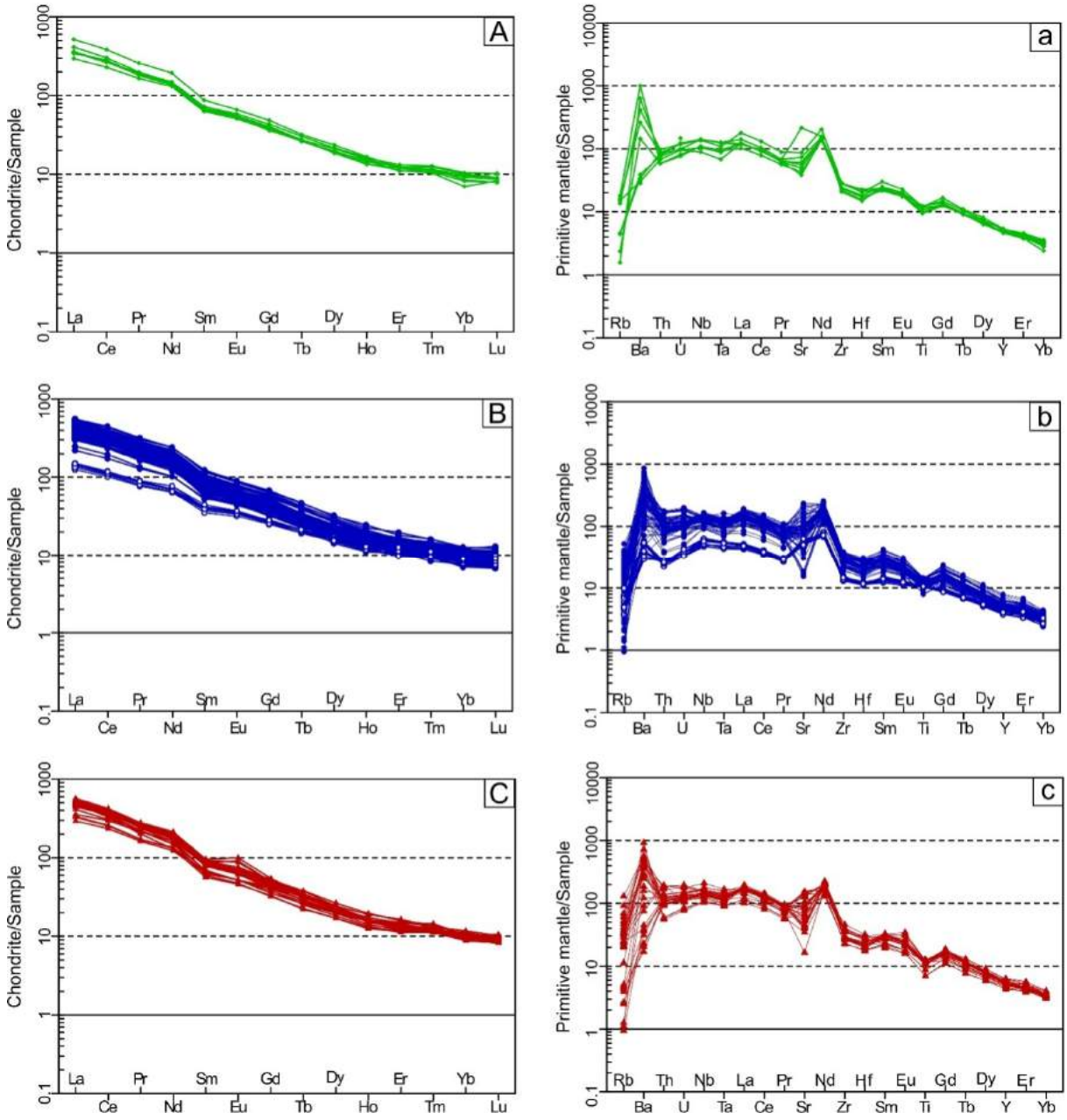

Figure 11. Chondrite normalized after McDonough & Sun (1995), Primitive mantle normalized after Sun & McDonough (1989) spider diagrams for whole-rock; (A&a) Dykes, (B&b) Sills and (C&c) Laccoliths.

2017). They share also negative anomalies in Sr and Ti indicating plagioclase and ferro-titane oxides fractionations (Fig.11). On the other hand, the negative anomalies in K and Rb are probably related to the fusion source, which suggest the presence of a phlogopite mantle (Ngounouno *et al*. 2006). It seems clear that TMC have slight geochemical variations, the parallelism of their profiles indicates that they probably come from the same deep source (Fig. 11). The concentration of some elements *versus* Zr (Fig. 12) shows a clear differentiation trend. Group 1 sills appear the least differentiated compared to the other components of the TMC.

Magmatic source

The TMC is enriched in light REE with respect to heavy REE with no Eu-anomalies (Fig. 11). This is clearly different from the typical N-MORB diagrams, but similar to the OIB (Oceanic Island Basalt) or IAB (Island Arc Basalt) and typical pattern of alkali basalts. They do not display a negative HFSEs anomaly (K, Sr and Th), similar to those of CFBs (continental flood basalt). The Ti/Y ratio is constant during fractional crystallization (Peat *et al.* 1992), generally used to discriminate the rock type (Xu *et al.* 2001, Xiau *et al.* 2004, Lai *et al.* 2012). The TMC have generally high TiO_2 composition (Tableau) with Ti/Y ratios higher than 500. In Ti/Y vs. Mg # and Ti/Y vs. Sm/Yb plots (Lai *et al.* 2012), the rocks are located in the field of Ti-rich basalts (Fig. 13). The TMC rocks plot in the field of MORB-OIB in the Nb/Yb *versus* Zr/Y diagram (Fig. 14C). The Yb vs La/Yb plot indicates that TMC have a trend of partial melting and is less evolved compared to fractional crystallization. A garnet source is suspected if $(Gd/Yb)_C > 2$

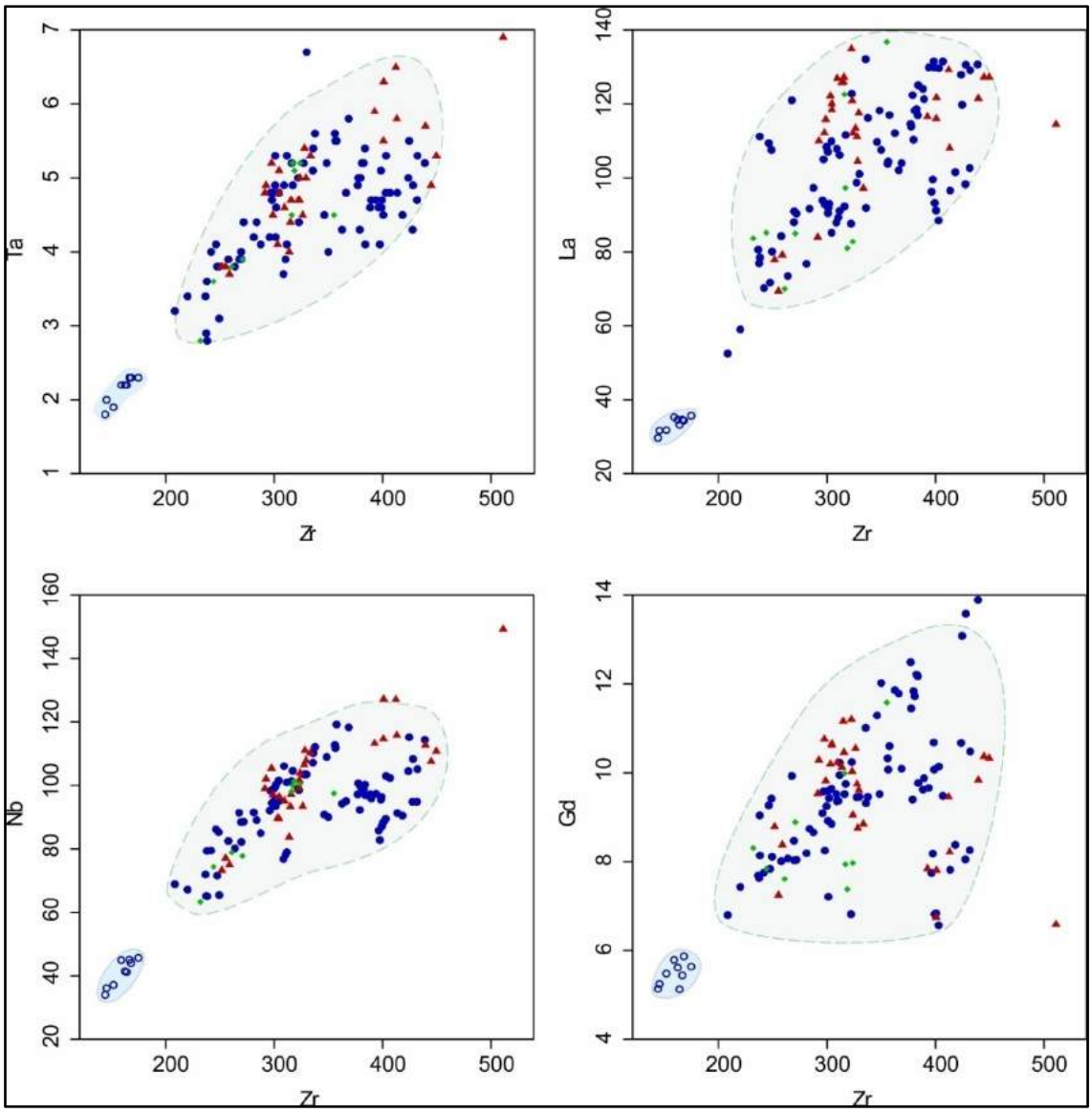

Figure12. Whole-rock co-variation diagrams for selected elements Ta, La, Nb, Gd vs Zr (symbols as Fig. 10).

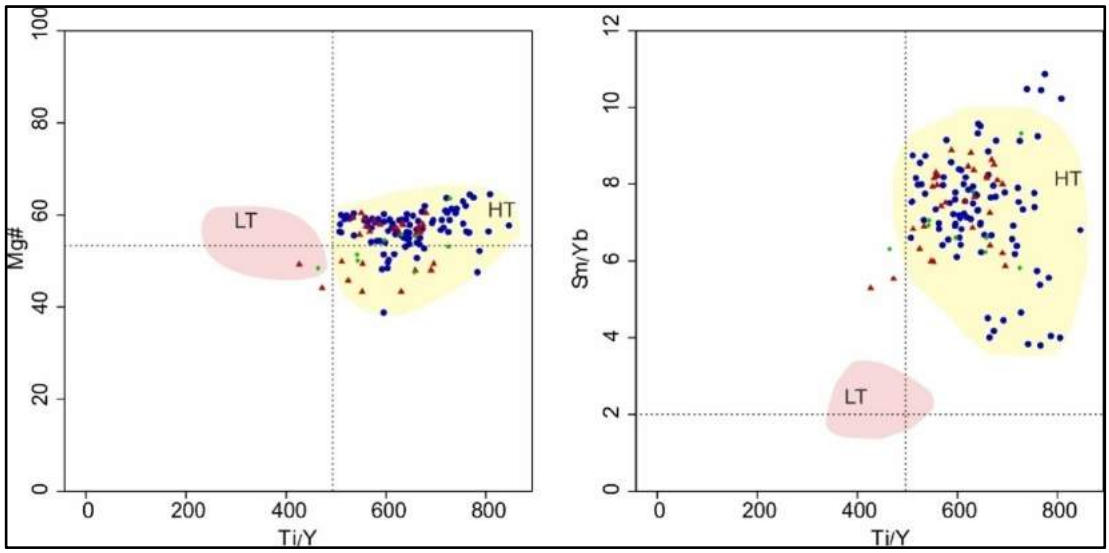

Figure13. Ti/Y vs.Mg# and Ti/Y vs. Sm/Yb diagrams after Lai *et al*. (2012) for the TMC, LT: Low-Ti; HT: High-Ti.

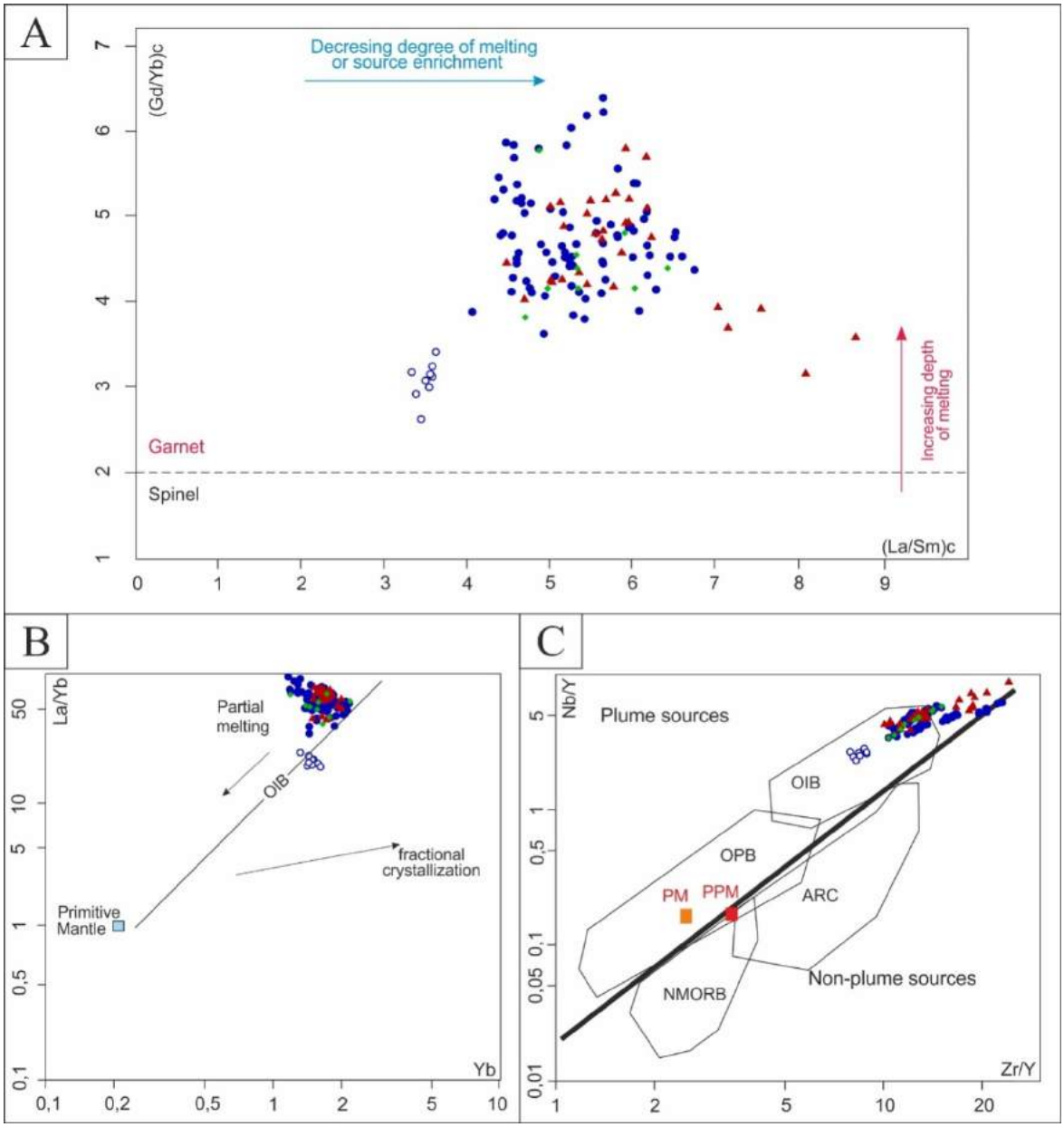

Figure 14. La/Sm vs. Sm/Yb, Yb vs. La/Yb, and Nb/Y vs. Zr/Y, diagrams to determine the possible mantle sources and the partial melting degrees of sources.(A) & (B) after Rooney (2010). Normalization values of the chondrite C after Sun & McDonough (1989). (C) after Condie (2005).

or $(Tb/Yb)_C$> 1.8 (Rooney 2010, Álvaro *et al*. 2014b). In the diagram $(La/Sm)_C$ vs $(Gd/Yb)_C$, the TMC is in the garnet source domain, indicating a genesis at a deeper source of asthenospheric mantle and confirm the conclusions obtained by Álvaro *et al*. (2014c). This diagram indicates as well that the olivine dolerites - group 1 sills are distinguished from the kaersutite lamprophyres - group 2 sills by a higher degree and lower depth of melting. The La/Ta and La/Nb ratios are generally used to distinguish between a lithospheric and asthenospheric mantle source, and the higher values are devoted to those of a lithospheric source with La/Ta> 22 and La/Nb> 1.8 (Coish & Sinton 1992). The TMC La/Ta ratio is between 15 and 31.45 (average 22.22). The ratio La/Nb is from 0.76 to 1.5, (average 1.80). These values are indicative for an asthenospheric to sub-lithospheric mantle source for the TMC. According to the Zr/Y vs. Nb/Y diagram of Condie (2005), the TMC rocks are located in the OIB plume source (Fig. 14). The Zr/Y and Nb/Y ratios are used by Fitton et al. (1997) to characterize the mantle plume source. Zr and Nb are trace elements and have similar properties during mantle melting while Y is slightly incompatible with Zr and Nb. Thus, different partial melting degrees of the same peridotite source should produce different basalt's evolution trend (Xijun *et al*. 2016). The TMC rocks display a ratio in Zr/Y between 7.94 and 24.10, in Nb/Y between 1.94 and 7.04. The ΔNb TMC's after Fitton *et al*. (1997) is mostly greater than 0, corresponding to the evolution field of Icelandic basalts and the plume source domain.

Tectonic setting

In the Nb/Yb -Th/Yb diagram, all TMC magmatic rocks are located in the MORB-OIB field (Fig. 15A). They present high Nb (91ppm average) and Zr (321ppm average) contents

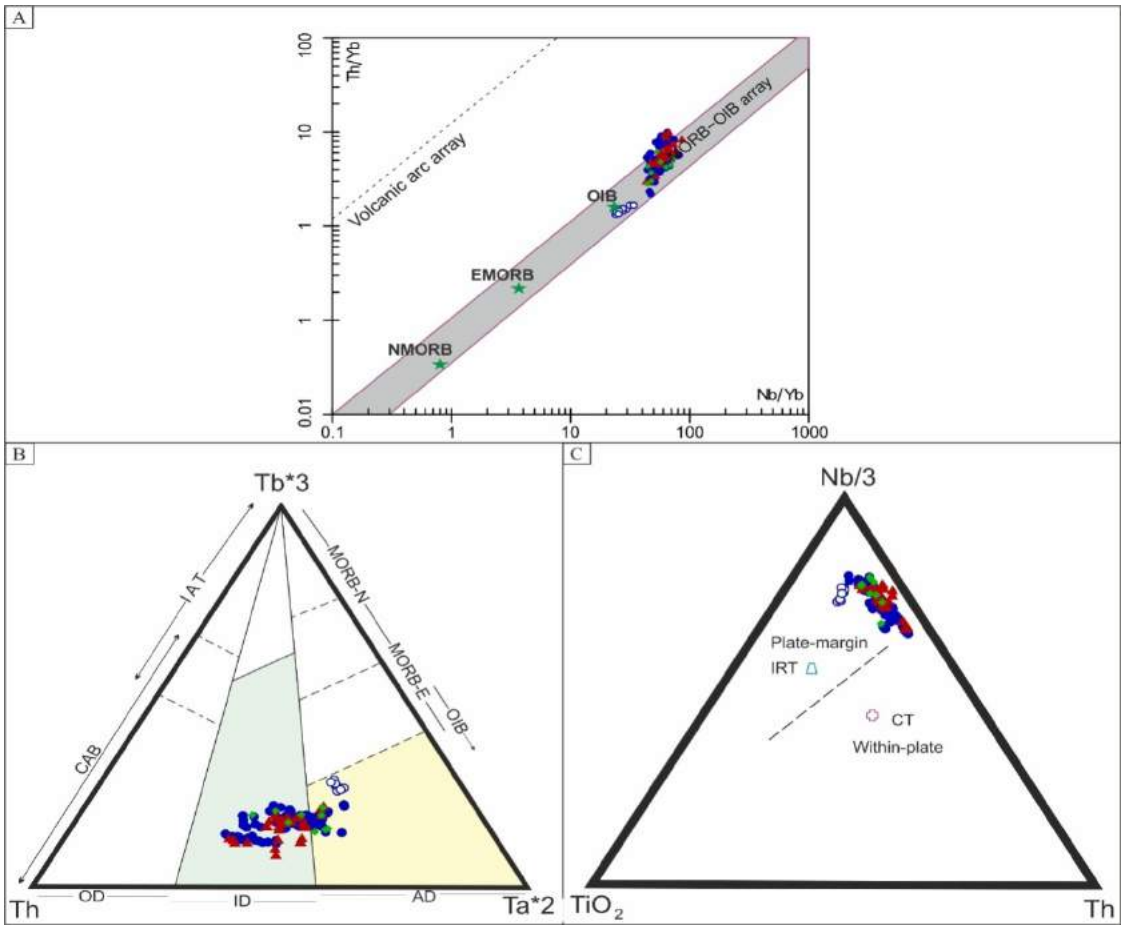

Figure15. (A) Nb/Yb vs Th/Yb diagram and (B) Nb/Yb vs TiO_2/Yb diagram after Pearce (2008), (C) Th-Tb*3-Ta*2 (OD: Orogenic domain, ID: Intermediate domain, AD: Anorgenic domain and (D) TiO_2-Nb/3-Th diagrams after Cabanis & Thiéblemont (1998) and Holm (1985). IRT : Initial Rift Tholeiite average after Pouclet *et al*. (1995), CT : Continental Tholeiite average after Holm (1985).

similar to those of OIB (Nb=48ppm) and Zr (280ppm) indicating an origin from an enriched mantle source (Sun & McDonough 1989). On the diagram Th-Tb.3-Ta.2, TMC rocks are spread in the continental tholeiitic domain and a part in the OIB field (Fig. 15C). In the Nb/3-TiO2-Th diagram, these rocks correspond to plate margin lavas (Fig. 15D), this diagram also confirms the initial tholeiitic rift character for the whole TMC in referring to the index proposed by Pouclet *et al*. (1995). According to these geochemical data, the TMC was set up in an extensive context probably controlled by the presence of a plume with slightly varying degrees of melting and probably different source depths.

DISCUSSION & CONCLUSION

Our approach allows us to distinguish a main family of rocks, the kaersutite lamprophyres recorded in dykes, laccoliths and sills. The olivine dolerites form a second family of rocks seen only in certain sills. There are only slight differences between these rock families or facies groups. They present the same mineralogical composition with olivine, pyroxene, kaersutite and plagioclase. Their geochemical signatures are similar with only minor differences. The TMC rocks consist of rich-Ti alkali basalts generated from asthenospheric to sub-lithospheric mantle probably controlled by the presence of a plume with slightly varying degrees of melting at slightly different depths. This magmatism took place in an intraplate extensive context.

The Ti/Y ratio greater than 500 is a predominant character in the basalts of the large LIP magmatic provinces (Xu *et al*. 2001, 2004, Zhong *et al*. 2006, Wang *et al*. 2011, Zhang *et al*. 2013, Lai *et al*. 2016). Generally, in the ratio Ti/Y, Ti shows a strong incompatibility with garnet ($D^{Ti}_{melt/garnet}$= 0.29, Johnson 1998). Whereas Y has a strong compatibility with the garnet ($D^{Y}_{melt/garnet}$= 4.2 – 7.1, Jenner *et al*. 1993). Therefore, high Ti/Y ratios indicate a deep partial melting where the garnet is stable, whereas low Ti/Y ratios correspond to partial melting in shallow-levels where the spinel is stable. The TMC rocks have an average Ti/Y ratio higher than 500. They are hence classified as Ti-rich basalts and originated from a garnet source deep plume.
The combination of regional geology with tectonics leads us to explain the generation of Ti/Y-rich rocks of TMC as follows. The Tafilalt sedimentary sequence (Robert-Charrue & Burkhard 2008, Baidder *et al*. 2016) and geophysical data (Robert-Charrue 2006) show that the region is characterized by a thick lithosphere and expressed insignificant uplift during the Paleozoic and the Mesozoic. The rise of a warm plume from the deep mantle triggered the partial melting of metasomatic veins and reservoirs in the continental Tafilalt lithosphere. The depth of the source and the variation of the

melting rate gave rise to two liquids different by their TiO_2 richness. A first minor poor TiO_2 liquid gave olivine dolerites. A second major rich TiO_2 liquid gave kaersutite lamprophyres rocks.

Pouclet *et al*. (2017) argued that the TMC rocks were folded and metamorphosed during the Late Carboniferous tectonic phases of the Variscan Orogeny. They suggest that their emplacement occurred during two distinct magmatic events, i) in the late Famennian- Tournaisian (for example the Znaigui and Dboa sites) and ii) in the early to late Visean (Eastern Mfis and Widane Chebbi), similar to what is observed in the Meseta realm. (Aarab & Beauchamp 1987, Kharbouch 1994, Roddaz *et al*. 2002, Bennouna *et al*. 2004, Driouch *et al*. 2010). However, all field arguments agree for intrusive emplacement in the Paleozoic folded units at least after the Visean, such as, (i) the fact that the feeder dykes cut across all Paleozoic terranes (inclusively the Visean); (ii) the presence of sill's frozen edges and laccoliths's cooling borders, and (iii) the absence of pillow-lavas and of sediment-lava interaction figures. In this scheme, it is very difficult, even inconceivable, to imagine the magmatic body of Znaigui as an underwater volcanic plug as proposed by Pouclet *et al*. (2017). It is simply an eroded, small growing laccolith, in concordance with the absence of coarse grained rocks (gabbros and syenites).

Chabou *et al*. (2017a-b) suggested a single event that would be much more recent in the Paleozoic-Mesozoic transition or even linking the complex to the presages of the opening of the Central Atlantic. Regionally, several dykes and doleritic sills are recognized in the West African domain and dated around 200 Ma. They belong to the Central Atlantic Magmatic Province (CAMP; Hailwood & Mitchell, 1971, Salmon *et al*. 1986, Knight *et al*. 2004, Chabou *et al*. 2007, 2008). Chabou *et al*. (2017a-b) used the immobile element-based discrimination diagram (Zr/Ti vs Nb/Y) to deduce the divergence of the TMC composition with respect to the CAMP field. In addition, the Ti (> 2 wt%) content of the TMC rocks does not match the tholeiitic Ti (<2 wt%) of the CAMP. The REE high-Ti tholeiitic CAMP basalts present flat REE patterns (Chabou *et al*. 2007), that don't fit with the TMC patterns.

In the Hoggar, doleritic dykes and sills intrude the lower Ordovician-Devonian formations in the Tim Mersoi Basin (Lessard 1961). They were attributed to Tournaisian by K/Ar (Djellit *et al*. 2006). In the Murzuq Basin, Derder *et al*. (2016) dated the same bodies by K/Ar to Praguian (410 Ma) with a rejuvenation at Serpukhovian (326 Ma). Recently, Mekkaoui *et al*. (2017) reported two geochemical signatures in dolerites from the Daoura-Ougarta Range, one being similar to those of the TMC and the other one to those of the CAMP. They would be therefore derived from two different mantle sources, through different melting conditions and subjected to distinct differentiation and contamination processes.

The northern margin of the Saharan platform housed several magmatic events between the latest stages of the Variscan evolution and the earliest stages of the Alpine Wilsonian cycle. The TMC magmatism is post-Visean, and then cannot be assigning to any of the Devonian or Carboniferous events known in the Meseta or Saharan domains. On the other hand, the TMC cannot be geochemically correlated with CAMP. This rationale leads to the assignation of the TMC to some specific event between the latest Paleozoic and the Late Triassic.

ACKNOWLEDGEMENTS

We are grateful to Prs. André Michard and Hassan El Hadi for their valuable comments and suggestions that led to numerous improvements in the paper quality, clarity and the English text. We also thank the two reviewers for their help and constructive remarks.

REFERENCES

Aarab E.M. & Beauchamp J. 1987. Le magmatisme carbonifère pré-orogénique des Jebilet Centrales (Maroc). Précisions pétrographiques et sédimentologiques. Implications géodynamiques. *Comptes. Rendus de l'Académie des Sciences. Paris*, 304, II, 169-174.

Alvaro J.J., Benharref M., Amrhar M. *et al*. 2014a. Carte géologique du Maroc 1/50 000, feuille de Al Atrous. *Notes et Mémoires du Service Géologique du Maroc*, 551.

Álvaro J.J., Aretz M., Benharref M. *et al*. 2014b. Carte géologique du Maroc au 1/50 000, feuille Tawz - Mémoire explicatif. *Notes et Mémoires du Service Géologique du Maroc*, 555bis.

Álvaro J.J., Pouclet A., Ezzouhairi H. *et al*. 2014c. Early Neoproterozoic rift-related magmatism in the Anti-Atlas margin of the West African craton, Morocco. *Precambrian Research*, 255, 433-442.

Baidder L. 2007. *Structuration de la bordure septentrionale du craton ouest africain du Cambrien à l'Actuel : cas de l'Anti-Atlas oriental*. Doctorat d'Etat. Hassan II University, Faculty of Sciences Aïn Chok, Casablanca, Morocco, 218 p.

Baidder L., Raddi Y., Tahiri M. *et al*. 2008. Devonian extension of the Pan-African crust north of the West African Craton, and its bearing on the Variscan foreland deformation: evidence from eastern Anti-Atlas (Morocco). In: Ennih, N., Liegeois, J.P. (Eds.), The Boundaries of the West African Craton, vol. 297. *Geological. Society London, Special. Publication*., 453-465.

Baidder L., Michard A., Soulaimani A. *et al*. 2016. Fold interference pattern in thick-skinned tectonics; a case study from the External Variscan Belt of Eastern Anti-Atlas, Morocco. *Journal of African Earth Sciences*, 119, 204-225.

Bellieni G., Picirillo E.M., Cavazzini G. *et al*. 1990. Low- and high TiO2, Mesozoic tholeiiticmagmatism of the Maranhão basin (NE-brazil): K‑Ar age, geochemistry, petrology,isotope characteristics and relationships with Mesozoic low- and high TiO2 floodbasalts of the Paraná Basin (SE-Brazil). Neues Jahrbuch. *Mineralogischer Abhandlungen*, 162, 1-33.

Benharref M., Alvaro J-J., Jmili A. *et al*. 2014a. Carte géologique du Maroc au 1/50 000, feuille Marzouga. *Notes et Mémoires du Service Géologique du Maroc*, 553.

Benharref M., Alvaro J-J., Hibti M. *et al*. 2014b. Carte géologique du Maroc au 1/50 000, feuille Marzouga, Mémoire explicatif, *Notes et Mémoires du Service Géologique du Maroc*, 553bis.

Benharref M., Álvaro J.-J, Pouclet A. *et al*. 2014c. Carte géologique du Maroc au 1/50 000, feuille Al Atrous, Mémoire explicatif. *Notes et Mémoires du Service Géologique du Maroc*, 551bis.

Benharref M., Hibti M., Pouclet A. *et al*. 2014d. Carte géologique du Maroc au 1/50 000, feuille Mfis, Mémoire explicatif. *Notes et Mémoires du Service Géologique du Maroc*, 554bis.

Bennouna A., Ben Abbou M., Hoepffner C. *et al*. 2004. The Carboniferous volcano-sedimentary depocentre of Tazekka Massif (Middle-Atlas, Morocco): new observations. *Journal of African Earth Sciences*, 39, 359-368.

Cébria J.M., Lopez-Ruiz J., Doblas M. *et al*. 2003. Geochemistry of the Early Jurassic Messejana-Plasencia dyke (Portugal-Spain) ; Implications on the Origin of the Central Atlantic Magmatic Province. *Journal of Petrology*, 44, 3, 547-568.

Chabou M.C., Sebaï A., Feraud G. *et al*. 2007. Datation $^{40}Ar/^{39}Ar$ de la Province Magmatique de l'Atlantique Central dans le Sud-Ouest algérien. *Comptes Rendus Geoscience*, 339, 970-978.

Chabou M.C. 2008. *Datation 39Ar-40Ar et Géochimie de la Province Magmatique de l'Atlantique Central dans le Sud-Ouest algérien. (40Ar/39Ar dating and Geochemistry of the Central Atlantic Magmatic Province (CAMP) in south western Algeria)*. PhD thesis. Ecole Nationale Polytechnique, Alger, 266p.

Chabou M.C. 2016. *Les ophites et spilites du Trias de la chaîne des Maghrébides et du domaine Atlasique du Nord-Est de l'Algérie et de la Tunisie : témoins de la CAMP ou épisode magmatique différent ? Contraintes géochimiques et paléogéographiques*. 1er Coll. Int. Géol. Chaînes Maghrébines, Sétif, Algeria, 65-68.

Chabou M.C., Michard A., Najih A. *et al*. 2017a. The Tafilalt dolerites (Morocco): Triassic camp or Devonian platform dislocation or else? A geochemical diagram helps to discard the camp. *1st International ASRO Geological Congress*, El Jadida, Morocco, 30-31.

Chabou M.C., Michard A., Fekkak A. *et al*. 2017b. The Tafilalt Magmatic check-point (Morocco) at the border of the "CAMP". *1st West African Craton and Margins International Workshop*, Dakhla, Morocco, Abstr., 35-36.

Chauvel C., Hofmann A.W. & Vidal P. 1992. HIMU-EM: the French Polynesian connection. *Earth and Planetary Science Letters*, 110, 99-119.

Choubert G. 1943. Quelques réflexions sur la terminaison orientale de l'Anti-Atlas. *Bulletin de la Société des Sciences Naturelles du Maroc*, 67-79.

Coish R.A. & Sinton C.W., 1992. Geochemistry of mafic dikes in the Adirondack Mountains: implications for Late Proterozoic continental rifting. Contributions to Mineralogy and Petrology, 110, 500-514.

Condie K.C. 2005. High field strength element ratios in Archean basalts: a window to evolving sources of mantle plumes? *Lithos*, 79, 491-504.

Cox K.G., Bell J.D. & Pankhurst R.J. 1979. The interpretation of igneous rocks. *London: G. Allen and Unwin*. 450p.

Davies J., Marzoli A., Bertrand H. *et al*. 2017. End-Triassic extinction started by intrusive CAMP activity. *Nature Communications*, 8, 15596.

Deckart K., Bertrand H. & Liégeois J.P. 2005. Geochemistry and Sr, Nd, Pb isotopic composition of the Central Atlantic Magmatic Province (CAMP) in Guyana and Guinea. *Lithos*, 82, 289-314.

De LaRoche H., Leterrier J., Grandclaude P. *et al*. 1980. A classification of volcanic and plutonic rocks using R1R2 - diagram and major element analyses - Its relationships with current nomenclature. *Chemical Geology*, 2, 183-210.

DeMin A., Piccirillo E.M., Marzoli A. *et al*. 2003. The Central Atlantic Magmatic Province (CAMP) in Brazil : Petrology, Geochemistry, $^{40}Ar/^{39}Ar$, Paleomagnestism and Geodynamic Implications. *American Geophysical Union*, 96-128.

Derder M.M.M., Maouche S., Liégeois J.P. *et al*. 2016. Discovery of a Devonian mafic magmatism on the western border of the Murzuq basin (Saharan metacraton): Paleomagnetic dating and geodynamical implications. *Journal of African Earth Sciences*, 115, 159-176.

Destombes J. & Hollard D. 1986. Carte géologique du Maroc au 1:200 000. Feuille Tafilalt-Taouz, *Notes et Mémoires du Service Géologique du Maroc*, 244.

Djellit H., Bellon H., Ouabadi A. *et al*. 2006. Age $^{40}K/^{40}Ar$, Carbonifère inférieur, du magmatisme basique filonien du synclinal paléozoïque de Tin Serririne, Sud-Est du Hoggar (Algérie). *Comptes Rendus Geosciences*, 338, 624-631.

Driouch Y., Béziat D., Grégoire M. *et al*. 2010. Clinopyroxene trace element compositions of cumulate mafic rocks and basalts from the Hercynian Moroccan Central Meseta: petrogenetic implications. *Journal of African Earth Sciences*, 56, 97-106.

Dupuy C., Marsh J., Dostal J. *et al*. 1988. Asthenospheric and lithospheric sources for Mesozoic dolerites from Liberia (Africa) : trace element and isotopic evidence. *Earth and Planetary Science Letters*, 87, 100-110.

Eisele J., Sharma M., Galer S.J.G. *et al*. 2002. The role of sediment recycling in EMI inferred from Os, Pb, Hf, Nd, Sr isotope and trace element systematics of the Pitcairn hotspot. *Earth and Planetary Science Letters*, 196, 3-4, 197-212.

Fitton J.G., Saunders A.D., Norry M.J. *et al*. 1997. Thermal and chemical structure of the Iceland plume. *Earth and Planetary Science Letters*, 153, 197-208.

Hailwood E.A. & Mitchell J.G. 1971. Paleomagnetic and radiometric dating results from Jurassic intrusions in South Morocco. Geophys. J. R. Astr. Soc. 24, 351-364.

Hofman A.W., Jochum K.P., Seufert M. *et al*. 1986. Nb and Pb in oceanic basalts: new constraints on mantle evolution. *Earth and Planetary Science Letters*, 79, 33-45.

Hofmann A.W. & White W.M. 1982. Mantle plumes from ancient oceanic crust. Earth and Planetary Science Letters 57, 421-436.

Hofmann, A.W. 1997. Mantle geochemistry: the message from oceanic volcanism. *Nature*, 385, 219-229.

Hollard H. 1974. Recherche sur la stratigraphie des formations du Dévonien moyen, de l'Emsien supérieur au Frasnien, dans le Sud du Tafilalt et dans le Maider (Anti-Atlas oriental, Maroc). *Notes et Mémoires du Service Géologique du Maroc*, 264, 7-68.

Hollard H. 1981. Principaux caractères des formations dévoniennes de l'Anti-Atlas. *Notes et Mémoires du Service Géologique du Maroc*, 308, 15-21.

Holm, P.E. 1985. The geochemical fingerprints of different tectonomagmatic environments using hygromagmatophile element abundances of tholeiitic basalts and basaltic andesites. *Chemical Geology*, 51, 303-323.

Jenner G.A., Foley S.F., Jackson S.E. *et al*. 1993. Determination of partition coefficients for trace elements in high pressure temperature experimental run products by laser ablation microprobeinductively coupled plasma-mass spectrometry (LAM-ICP-MS). *Geochimica et Cosmochimica Acta*, 57, 5099-5103.

Johnson M.K.T. 1998. Experimental determination of partition coefficients for rare earth and high-field-strength elements between clinopyroxene, garnet, and basaltic melt at high pressures. *Contributions to Mineralogy and Petrology, 1*33, 60-68.

Kharbouch F. 1994. Le volcanisme devono-dinantien du Massif central et de la Meseta orientale. *Bulletin de l'Institut Scientifique, Rabat*, Maroc. 18, 192-200.

Koukaya A., Amrhar M., Tahiri A. *et al*. 2014. Carte géologique du Maroc au 1/50 000, feuille de Tawz. *Notes et Mémoires du Service Géologique du Maroc*, 555.

Knight K.B., Nomade S., Renne P.R. *et al*. 2004. The Central Atlantic Magmatic Province at the Triassic-Jurassic boundary : paleomagnetic and 40Ar/30Ar evidence from Morocco from brief, episodic volcanism. *Earth and Planetary Science Letters*, v.288, 143-160.

Lai S., Qin J., Li Y. *et al*. 2012. Permian high Ti/Y basalts from the eastern part of the Emeishan Large Igneous Province, southwestern China : Petrogenesis and tectonic implications. *Journal of Asian Earth Sciences*, 47, 216-230.

Lessard L. 1961. Les sériesprimaires des Tassilis Oua-n-Ahaggar au sud du Hoggar entre l'Aïr et l'Adrar des Iforas (Sahara méridional). *Bulletin de la Société Géologique de France*, 7, 3, 501-513.

Liu X., Liang Q., Li Z. *et al*. 2017. Origin of Permian extremely high Ti/Y mafic lavas and dykes from Western Guangxi, SW China : Implications for the Emeishan mantle plume magmatism. *Journal of Asian Earth Sciences*, 141, 97-111.

Marzoli A., Bertrand H., Knight K.B. *et al*. 2004. Synchrony of the Central Atlantic magmatic province and the Triassic-Jurassic boundary climatic and biotic crisis. *Geology*, 32, 973-976.

McDonough W.F. & Sun S.S. 1995. The composition of Earth. *Chemical Geology*, 120, 228.

Mekkaoui A., Bénaouda N.R. & Tazerout K.G. 2017. Mafic dikes at Kahel Tabelbala (Daoura, Ougarta Range, south-western Algeria):

New insights into the petrology, geochemistry and mantle source characteristics. *Comptes Rendus Geoscience*, 349, 5, 202-211.

Merle R., Marzoli A., Bertrand H. *et al*. 2011. $^{40}Ar/^{39}Ar$ ages and Sr-Nd-Pb-Os geochemistry of CAMP tholeiites from Western Maranhão basin (NE Brazil). *Lithos*, 122, 137-151.

Michard A., Soulaimani A., Ouanaimi H. *et al*. 2017. Saghro Group in the Ougnat Massif (Morocco), an evidence for a continuous Cadomian basin along the northern West African Craton. *Comptes Rendus Geoscience*, 349, 2, 81-90.

Michard A., Soulaimani A., Hoepffner C. *et al*. 2010. The south-western branch of the Variscan Belt: evidence from Morocco. *Tectonophysics*, 492, 1-24.

Middlemost E.A.K. 1989. The basalt clan. *Earth Science Revue*, 11, 4, 337-364.

Ngounouno I., Déruelle B., Montigny R. *et al*. 2006. Les camptonites du mont Cameroun, Cameroun, Afrique. *Comptes Rendus Geoscience*, 338, 537-544.

Niu Y.L. 2009. Some basic concepts and problems on the petrogenesis of intra-plate ocean island basalts. *Chinese Science Bulletin*, 54, 4148-4160.

Pearce J.A., 2008. Geochemical fingerprinting of oceanic basalts with applications to ophiolite classification and the search for Archean oceanic crust. *Lithos*, 100, 14-48.

Peate D.W., Hawkesworth C.J. & Mantovani M.S.M., 1992. Chemical stratigraphy of the Parani lavas (South America): classification of magma types and their spatial distribution. *Bulletin of Volcanology*, 55, 119-139.

Pe-Piper G. & Reynolds P.H. 2000. Early Mesozoic alkaline mafic dykes, southwestern Nova Scotia, Canada, and their bearing on Triassic-Jurassic magmatism. *Canadian Mineralogist*, 38, 217-232.

Pilet S., Baker M.B. & Stolper E.M. 2008. Metasomatized lithosphere and the origin of alkaline lavas. *Science*, 320, 916-919.

Pouclet A., Lee J.S., Vidal P. *et al*. 1995. Cretaceous to Cenozoic volcanism in South Korea and in the Sea of Japan : magmatic constraints on the opening of the back-arc basin. In: Smellie, J.L. (Ed.), Volcanism Associated with Extension at Consuming Plate Margins, vol. 81. *Geological Society London Special Publications*, 169-191.

Pouclet A., El Hadi H., Bardintzeff J-M. *et al*. 2017. Devonian to Early Carboniferous magmatic alkaline activity in the Tafilalt Province, Eastearn Morocco: An Eovariscan episode in the Gondwana margin, north of the West African Craton. *Journal of African Earth Sciences*, 129, 814-841.

Robert-Charrue C. & Burkhard M. 2008. Inversion tectonics, interference pattern and extensional fault-related folding in the Eastern Anti-Atlas, Morocco. *Swiss Journal of Geosciences*, 101, 397-408.

Robert-Charrue C. 2006. *Géologie structurale de l'Anti-Atlas oriental, Maroc*. Ph.D. Thesis. Univ. Neuchâtel, 180 p.

Roddaz M., Brusset S., Soula J.-C. *et al*. 2002. Foreland basin magmatism in theWestern Moroccan Meseta and geodynamic inferences. *Tectonics*, 21, 1043-1065.

Rooney T.O. 2010. Geochemical evidence of lithospheric thinning in the southern Main Ethiopia Rift. *Lithos*, 117, 33-48.

Salmon E., Montigny R., Edel J.B. *et al*. 1986. A 140Ma K/Ar age for the Msissi norite (Morocco): new geochemical and paleomagnetic data. *Earth and Planetary Science Letters*, 81, 265-272.

Sebai A., Féraud G., Bertrand H. *et al*. 1991. $^{40}Ar/^{39}Ar$ dating and geochemistry oftholeiitic magmatism related to the early opening of the Central Atlantic rift. *Earth and Planetary Science Letters*, 104, 455‑472.

Shellnutt J.G. & Jahn B.M. 2011. Origin of Late Permian Emeishan basaltic rocks from the Panxi region (SW China): Implications for the Ti-classification and spatial–compositional distribution of the Emeishan flood basalts. *Journal of Volcanology and Geothermal Research*, 199, 85-95.

Soulaimani A. & Burkhard M. 2008. The Anti-Atlas chain (Morocco): the southern margin of the Variscan belt along the edge of the West African craton. In: Ennih, N., Liegeois, J.-P. (Eds.), The boundaries of the West African craton, *Geological Society of London Special Publications*, 279, 433-452.

Sun S.S. & McDonough W.F. 1989. Chemical and isotopic systematics of oceanic basalts: implications for mantle composition and processes. *Geological Society Geological Society, London, Special Publications*, 42, 313-345.

Tahiri A., Belfoul A., Benharref M. *et al*. 2014. Carte géologique du Maroc 1/50 000, feuille Mfis. *Notes et Mémoires du Service Géologique du Maroc*, 554.

Takahashi E., Nakajima K. & Wright T.L. 1998. Origin of the Columbia River basalts: melting model of a heterogeneous plume head. *Earth and Planetary Science Letters*, 162, 63–80.

Taylor S.R. & McLennan S.M. 1985. The continental crust: its composition and evolution. *Blackwell Scientific Publication*, Carlton, 312.

Verati C., Rapaille C., Féraud G. *et al*. 2007. $^{40}Ar/^{39}Ar$ ages and duration of the Central Atlantic Magmatic Province volcanism in Morocco and Portugal and its relation to the Triassic-Jurassic boundary. *Palaeogeography, Palaeoclimatology, Palaeoecology*, 244, 308-325.

Wang C.Y., Zhou M.F. & Qi L. 2011. Chalcophile element geochemistry and petrogenesis of high-Ti and low-Ti magmas in the Permian Emeishan large igneous province, SW China. *Contributions to Mineralogy and Petrology*, 161, 237-254.

Wedepohl K.H. 1995. The composition of the continental crust. *Geochimica et Cosmochimica Acta*, 59, 1217-1232.

Wendt J. 1985. Disintegration of the continental margin of north-western Gondwana: late devonian of the eastern Anti-Atlas (Morocco). *Geology*, 13, 815-818.

Wendt J. 1988. Facies pattern and paleogeography of the middle and late Devonian in the eastern Anti-Atlas, Morocco. In: Mc Millan, N.J., Embry, A.F., Glass, D.G. (Eds.), Devonian of the World. *Canadian Society of Petroleum Geologists*, 14, 467-480.

White W.M. & Duncan R.A. 1996. Geochemistry and geochronology of the Society Islands: New evidence for deep mantle recycling. *American Geophysical Union Geophys Monogr*, 95, 183-206

Xiao L., Xu Y.G., Mei H.J. *et al*. 2004. Distinct mantle sources of low-Ti and high-Ti basalts from the western Emeishan large igneous province, SW China: implications for plume–lithosphere interaction. *Earth and Planetary Science Letters*, 228, 525-546.

Xu Y.G., Chung S.L., Jahn B.m. *et al.* 2001. Petrologic and geochemical constraints on the petrogenesis of Permian-Triassic Emeishan flood basalts in southwestern China. *Lithos* 58, 145-168.

Xu Y.G., He B., Chung S.L., et al. 2004. Geologic, geochemical, and geophysical consequences of plume involvement in the Emeishan floodbasalt province. *Geology*, 32, 917-920.

Xu Y.G., He B., Huang, X.L. *et al* 2007. Late Permian emeishan flood basalts in southwestern China. *Earth Science Frontiers*, 14, 1-9.

Youbi N., Tavares Martins L., Munha J.M. *et al*. 2003. The Late Triassic-Early Jurassic Volcanism of Morocco and Portugal in the framework of the Central Atlantic Magmatic Province : an overview.W.E. Hames, J.G. McHone, P.R. Renne, C. Ruppel (Eds.), The Central Atlantic Magmatic Province: Insights From Fragments of Pangea. *Geophysical Monograph Series*, 136, 179-207.

Zhang Z.C., Mahoney J.J., Mao J.W. et al. 2006. Geochemistry of picritic and associated basalt flows of the western Emeishan flood basalt province, China. *Journal of Petrology*, 47, 1997-2019.

Manuscrit reçu le 04/06/2018
Version révisée acceptée le 06/12/2018
Version finale reçue le 21/12/2018
Mise en ligne le 24/12/2018

Tableau. Chemical analyses of Tafilalt magmatic complex .

Sample	TA6	TA2	TA3	TA4	TA22	TA20	TA21
Location	Al Atrous				Oum Lhdej		
Hostrock	Silurian	Lochkovian			Givetian	Famennian	Famennian
Setting	Sill	Sill	Sill	Sill	Sill	Sill	Sill
Group	G2	G1	G1	G1	G2	G2	G2
(Wt%)							
SiO2	44.55	43.29	41.35	44.77	40.7	39.58	41.78
Al2O3	15.93	14.99	14.47	15	13.07	12.56	13.32
Fe2O3	8.49	11.12	11.05	11.96	12.43	12.24	12.43
MgO	5.23	7.2	6.09	7.82	6.66	6.34	7.01
CaO	7.8	8.53	10.47	7.1	9.37	9.96	9.74
Na2O	4.74	3.05	2.64	4.05	3.94	3.56	3.17
K2O	0.62	0.56	0.38	0.52	1.1	0.54	1.22
TiO2	2.07	2.24	2.26	2.3	3.05	3.02	3.13
P2O5	1.6	0.7	0.73	0.69	2.08	2.14	2.07
MnO	0.09	0.15	0.14	0.16	0.17	0.16	0.19
Cr2O3	0.013	0.021	0.017	0.021	0.01	0.01	0.01
LOI	8.4	7.8	10.1	5.3	6.5	9.3	5.2
Sum	99.57	99.69	99.72	99.68	99.06	99.45	99.27
(ppm)							
Ba	1040	368	266	381	1570	826	2317
Cs	2.2	1.1	2.6	0.6	20.9	3.4	0.4
Ga	20.4	18.4	17.9	18.1	19.5	19.6	19.4
Hf	7.6	3.5	3.4	3.6	8.6	8	8.4
Nb	82.8	34	36.2	37.2	98.8	94.3	97.2
Rb	11.9	4.4	2.4	6.3	18.1	7	12.2
Sn	2	1	2	2	2	2	3
Sr	935.5	1177.9	1093.2	1234.8	4413.8	2065.6	2089.6
Ta	4.1	1.8	2	1.9	5.2	4.3	4.9
Th	10.6	1.9	2.1	2.1	9.6	8.5	8.9
U	3.1	0.7	0.7	0.8	2.4	2.2	2.5
Zr	397.9	144.8	146.1	152.4	382.8	362.9	377.5
Y	19.2	17.5	17.2	17.1	29.6	27.3	27.7
La	99.6	29.7	31.7	31.8	118.6	112.1	114.6
Ce	190.8	61.9	67.2	65	243.7	238.3	244.4
Pr	19.23	7.32	7.59	7.56	27.4	26.61	26.63
Nd	69.5	30	30.8	30.6	104.4	99.4	102.6
Sm	10.37	5.4	6.03	5.76	16.04	15.52	15.75
Eu	2.96	1.84	1.96	1.95	4.65	4.46	4.58
Gd	8.18	5.14	5.25	5.48	12.21	11.86	12.49
Tb	0.98	0.72	0.76	0.75	1.57	1.52	1.5
Dy	4.9	3.82	4.09	3.73	6.86	6.97	6.9
Ho	0.73	0.72	0.67	0.71	1.14	1.03	1.12
Er	1.79	1.6	1.61	1.87	2.71	2.62	2.62
Tm	0.25	0.23	0.23	0.25	0.33	0.32	0.34
Yb	1.49	1.42	1.49	1.44	1.96	1.88	2.05
Lu	0.22	0.19	0.21	0.21	0.27	0.25	0.28

Sample	TA6	TA2	TA3	TA4	TA22	TA20	TA21
Location	Al Atrous				Oum Lhdej		

Hostrock	Silurian	Lochkovian			Givetian	Famennian	Famennian
Setting	Sill	Sill	Sill	Sill	Sill	Sill	Sill
Group	G2	G1	G1	G1	G2	G2	G2
(Wt%)							
SiO2	44.55	43.29	41.35	44.77	40.7	39.58	41.78
Al2O3	15.93	14.99	14.47	15	13.07	12.56	13.32
Fe2O3	8.49	11.12	11.05	11.96	12.43	12.24	12.43
MgO	5.23	7.2	6.09	7.82	6.66	6.34	7.01
CaO	7.8	8.53	10.47	7.1	9.37	9.96	9.74
Na2O	4.74	3.05	2.64	4.05	3.94	3.56	3.17
K2O	0.62	0.56	0.38	0.52	1.1	0.54	1.22
TiO2	2.07	2.24	2.26	2.3	3.05	3.02	3.13
P2O5	1.6	0.7	0.73	0.69	2.08	2.14	2.07
MnO	0.09	0.15	0.14	0.16	0.17	0.16	0.19
Cr2O3	0.013	0.021	0.017	0.021	0.01	0.01	0.01
LOI	8.4	7.8	10.1	5.3	6.5	9.3	5.2
Sum	99.57	99.69	99.72	99.68	99.06	99.45	99.27
(ppm)							
Ba	1040	368	266	381	1570	826	2317
Cs	2.2	1.1	2.6	0.6	20.9	3.4	0.4
Ga	20.4	18.4	17.9	18.1	19.5	19.6	19.4
Hf	7.6	3.5	3.4	3.6	8.6	8	8.4
Nb	82.8	34	36.2	37.2	98.8	94.3	97.2
Rb	11.9	4.4	2.4	6.3	18.1	7	12.2
Sn	2	1	2	2	2	2	3
Sr	935.5	1177.9	1093.2	1234.8	4413.8	2065.6	2089.6
Ta	4.1	1.8	2	1.9	5.2	4.3	4.9
Th	10.6	1.9	2.1	2.1	9.6	8.5	8.9
U	3.1	0.7	0.7	0.8	2.4	2.2	2.5
Zr	397.9	144.8	146.1	152.4	382.8	362.9	377.5
Y	19.2	17.5	17.2	17.1	29.6	27.3	27.7
La	99.6	29.7	31.7	31.8	118.6	112.1	114.6
Ce	190.8	61.9	67.2	65	243.7	238.3	244.4
Pr	19.23	7.32	7.59	7.56	27.4	26.61	26.63
Nd	69.5	30	30.8	30.6	104.4	99.4	102.6
Sm	10.37	5.4	6.03	5.76	16.04	15.52	15.75
Eu	2.96	1.84	1.96	1.95	4.65	4.46	4.58
Gd	8.18	5.14	5.25	5.48	12.21	11.86	12.49
Tb	0.98	0.72	0.76	0.75	1.57	1.52	1.5
Dy	4.9	3.82	4.09	3.73	6.86	6.97	6.9
Ho	0.73	0.72	0.67	0.71	1.14	1.03	1.12
Er	1.79	1.6	1.61	1.87	2.71	2.62	2.62
Tm	0.25	0.23	0.23	0.25	0.33	0.32	0.34
Yb	1.49	1.42	1.49	1.44	1.96	1.88	2.05
Lu	0.22	0.19	0.21	0.21	0.27	0.25	0.28

TA21+	TA46	TA48	TA52	TA53	TA54	TA55	TA56
Famennian	Mfis Famennian						
Sill	Sill	Laccolith	Laccolith	Laccolith	Laccolith	Laccolith	Laccolith
G2	G2	G2	G2	G2	G2	G2	G2
(Wt%)							
42.72	43.17	44	42.77	50.29	51.42	43.08	40.83

12.74	14.87	15.09	15.15	18.79	18.62	15.16	15.22
12.56	10.24	10.53	10.97	6.34	5.59	10.43	9.68
7.19	5.99	7.35	5.13	4.03	2.23	6.8	6.64
8.89	8.8	7.85	8.05	4.89	5.95	9.14	8.94
3.54	4.22	3.5	4.75	3.65	5.49	4.04	4.65
0.56	1.07	2.8	0.16	4.57	2.78	1.61	0.16
3.03	2.63	2.63	2.66	1.89	1.53	2.62	2.53
1.92	2.04	2.1	2.18	0.59	0.45	2.12	2.02
0.18	0.12	0.15	0.09	0.13	0.13	0.14	0.09
0.016	0.011	0.013	0.01			0.01	0.012
6	5.9	3.3	7.7	4	5.1	4.1	8.8
99.31	99.09	99.27	99.67	99.21	99.33	99.26	99.52
(ppm)							
2048	4142	1959	253	1933	1101	2837	159
0.4	0.7	8.7	0.3	0.3	1.2	0.4	0.3
19	19.5	19.6	18.5	20.3	21.2	19.3	19.5
7.9	6.7	6.6	6.7	8	8.1	6.3	6.3
90	98.5	89.7	95.2	113.3	114.7	97.2	96.4
5.1	10.4	29.8	3	43.8	26.4	18.4	2.5
3	2	2	4	2	2	2	3
2050.8	1968.4	2662.9	926.1	3188.1	2963.8	1932.9	839.5
4	4.4	4.1	4.6	5.9	5.5	4.7	4.8
8.5	8.6	8.4	8.8	9.8	11.5	8.4	7.8
2.3	2.6	2.5	2.7	3	3.1	2.4	2.6
350.3	323.1	303.1	309.5	392.5	400.7	315.7	304.5
28.4	23.6	23.4	23.1	20.7	19.4	23.6	27.1
107.6	122.8	122.2	126.9	116.6	116	127.2	118.5
224.9	233.2	239.9	241.1	214.4	200.2	239.3	224.5
24.84	24.14	24.38	24.86	21.02	19	24.68	22.93
95.7	90	90.9	90.5	70.3	60.6	90.5	85.3
14.9	13.33	13.63	13.29	10.55	8.64	13.21	13.49
4.29	3.95	3.93	5.28	2.98	2.67	3.84	4.42
12.02	10.24	10.2	10.23	7.85	6.75	10.46	10.62
1.51	1.21	1.22	1.2	0.95	0.83	1.22	1.3
6.7	5.66	5.6	5.67	4.62	4.31	5.79	5.98
1.06	0.95	0.91	0.9	0.76	0.71	0.91	0.91
2.54	2.13	2.12	2.11	1.85	1.93	2.15	2.17
0.36	0.26	0.28	0.29	0.28	0.27	0.29	0.28
1.93	1.74	1.6	1.66	1.76	1.56	1.82	1.69
0.23	0.24	0.25	0.24	0.25	0.25	0.21	0.24

TA57	TA58	TA61	TA62	TA64a	TA66	TA68	TA69
Laccolith G2	Laccolith G2	Laccolith G2	Laccolith G2	Laccolith G2	Laccolith G2	Laccolith G2	Laccolith G2
(Wt%)							
43.99	44.14	47.45	45.11	43.51	40.87	42.79	42.82
15.05	16.37	17.71	15.97	15.11	14.95	14.82	14.23
10.54	10.33	6.96	10.04	10.5	10.82	10.06	10.94
6.85	4.81	2.69	4.95	6.67	6.19	6.37	6.84

8.73	6.16	7.54	6.41	6.6	8.21	8.38	8.25
3.61	4.71	2.97	3.06	3.7	4.41	4.86	4.13
2.23	1.89	5.11	3.88	2.52	0.17	0.49	1.1
2.6	2.66	2.23	2.6	2.65	2.66	2.63	2.4
2.16	1.41	0.74	1.42	2.18	2.18	1.96	2.44
0.14	0.14	0.12	0.14	0.15	0.15	0.24	0.26
0.011	0.009		0.009	0.011	0.011	0.008	0.013
3.2	6.8	5.5	5.6	5.5	8.2	6.5	5.8
99.16	99.47	99	99.24	99.15	98.78	99.13	99.22
(ppm)							
2885	2558	3823	3840	2703	144	3849	3389
0.4	1	0.7	0.4	0.8	0.2	0.4	0.8
19.5	20.6	22.3	19.9	21.6	20.2	18.6	18.5
6.6	5.4	9	5.6	6.7	7.2	7.3	6.5
89.5	75	127.1	73.3	93.4	99.1	106.5	83.7
23.7	21.3	58.3	33.1	18.4	1.7	7.1	14.7
2	2	2	3	2	4	1	1
2782.5	730.3	3131.3	1373.7	2918.4	866.3	1915.6	1626
5.1	3.7	6.5	3.8	4.4	4.7	5.4	4
8.1	4.7	10.6	5	9.8	9.2	8.6	8.4
2.3	1.6	2.9	1.8	2.8	2.5	2.4	2.4
304.4	258.8	412.1	251.8	315	322.4	327.7	313.9
23.3	23.1	24.2	22.4	24.1	24.2	25	26
120.1	79.2	129.3	77.9	126	134.9	111.2	125.8
227.6	158	245	154.7	239.4	257.1	221.1	247.4
23.98	16.31	24.15	16.14	24.96	26.47	23.53	25.92
88	62.4	85.8	61.2	93.1	99.5	86.1	94.5
13.13	10.18	11.9	10.04	13.22	14.64	13.19	14.45
4.01	2.98	3.56	3.01	3.91	5.78	3.76	3.91
10.65	8.38	9.46	8.79	11.16	11.2	9.75	10.12
1.24	1.08	1.15	1.07	1.28	1.31	1.2	1.27
5.87	5.27	5.91	5.09	5.86	5.73	5.77	6.3
0.85	0.89	0.9	0.91	0.88	0.93	0.91	0.92
2.16	2.08	2.52	2.12	2.17	2.2	2.38	2.38
0.27	0.27	0.32	0.28	0.28	0.28	0.29	0.3
1.52	1.64	1.99	1.71	1.62	1.78	1.92	1.77
0.24	0.26	0.23	0.21	0.24	0.24	0.24	0.29

TA60	TA65	TA67	TA70	TA74	TA18	TA23a	TA23b
Dyke G2	Dyke G2	Sill G2	Dyke G2	Sill G2	Ouzina Famennian Dyke G2	Marzouga Tournaisian Sill G2	Sill G2
(Wt%)							
42.65	46.22	41.65	43.15	43.42	40.42	42.39	42.39
15.32	16.68	14.9	14.76	15.14	14.13	14.54	14.53
12.94	9.91	9.56	10.27	10	10.26	10.31	10.05
6.15	4.55	6.41	6.22	6.29	6.43	6.83	6.94
5.47	5.61	8.26	9.14	8.33	9.4	8.25	8.42
4.96	6.53	4.03	4.63	4.44	3.15	4.91	4.91

0.15	0.03	0.74	0.61	0.8	0.52	0.87	0.85
2.55	2.63	2.64	2.6	2.68	2.32	2.75	2.91
2.28	1.45	2.1	2.11	1.13	1.85	1.74	1.61
0.11	0.14	0.4	0.23	0.14	0.13	0.14	0.13
0.01	0.006	0.011	0.01	0.017	0.012	0.015	0.019
7	5.9	8.8	5.5	7.1	11.1	6.6	6.4
99.63	99.62	99.54	99.25	99.51	99.67	99.31	99.12
(ppm)							
198	1015	672	2890	1024	212	2478	4494
0.6	0.4	2.3	0.6	39.7	1.7	27.4	23.8
20.6	22	20.1	19.3	19.5	16.2	19.3	18.7
7.2	5.6	6.9	6.3	4.4	4.8	7	6.4
97.5	77.8	107.2	98.1	67.2	74.4	103.5	95.9
3.8	1.5	9.6	8.7	9.8	9.6	12.3	11
5	2	3	1	1	2	3	3
996.5	808.7	1531.7	1826.6	1778.2	1190.5	1851.6	1705.2
4.5	3.9	5.1	4.5	3.4	3.6	6.7	5.3
9.4	5	9	8.3	3.4	5.8	7.3	7
3.1	1.7	2.8	2.5	1.1	2	2.3	2.1
355.2	270.9	336.1	316.2	220.6	244.2	330.3	301.3
32.9	24	26.2	24.7	20.5	21.1	23.2	20.6
136.8	85	132.1	122.6	59	85.2	101.1	90.5
252.4	163.7	247.1	234.1	119.9	165.7	198.4	184.9
26.26	17.28	25.14	24.45	12.82	17.97	20.54	19.02
94.6	65.9	93.9	90.4	48.2	66.9	74.6	71.7
13.78	11.04	14.19	13.43	8.07	10.31	11.57	11.1
4.28	3.39	3.58	3.83	2.78	3.15	3.54	3.25
11.58	8.89	11.01	9.99	7.43	7.84	9.46	8.92
1.54	1.13	1.29	1.19	0.92	1.02	1.16	1.13
8.36	5.51	6.22	6	4.65	4.8	5.47	5.04
1.43	0.91	0.96	0.94	0.77	0.86	0.87	0.84
3.5	2.19	2.3	2.05	1.96	1.81	2.12	1.93
0.4	0.31	0.29	0.3	0.26	0.27	0.25	0.25
1.72	1.45	1.56	1.76	1.63	1.56	2.04	1.63
0.21	0.21	0.22	0.2	0.22	0.2	0.29	0.22

TA24	TA33
	Visean
Sill	Sill
G2	G2
(Wt%)	
42.22	42.48
14.37	13.84
10.43	11.99
7.32	7.03
8.35	7.6
4.58	3.83
0.7	0.89
2.86	2.99
1.65	1.72
0.15	0.15

0.019	0.014
6.7	6.7
99.35	99.19
(ppm)	
1999	2844
18.5	13.9
20.6	20.3
6.7	7.6
101.4	90.8
10.7	14.9
3	6
1945.6	2303.2
5.2	4.5
7.2	8.1
2.2	2.5
316.6	346.5
22.7	27.7
92.3	109.7
183.6	216.5
19.85	24.14
76.6	92.7
11.55	14.28
3.56	3.96
9.52	11.29
1.15	1.46
5.36	6.69
0.88	1.12
1.95	2.82
0.26	0.34
1.56	2.04
0.2	0.29